Linear and nonlinear rheological behavior of fat crystal networks

Braulio A. Macias-Rodriguez & Alejandro A. Marangoni

📅 Accepted author version posted online: 04 May 2017.

✎ Submit your article to this journal ☐

🔍 View related articles ☐

▣ View Crossmark data ☐
CrossMark

Linear and nonlinear rheological behavior of fat crystal networks

Braulio A. Macias-Rodriguez[a] and Alejandro A. Marangoni[*,a]

[a]Department of Food Science, University of Guelph, Guelph, Ontario, N1G 2W1, Canada

[*]Contect *E-mail*: amarango@uoguelph.ca

Abstract

Fats are ubiquitous in biological membranes, foods and many other commercial products. In these, they play essential roles in biological, nutritional and physical functions. In this review, we focus on physical mechanical functions. The rheology of fats arises from the crystal network, which displays hierarchical structural levels from the molecular to the mesoscopic. Under linear deformations, the crystal network behaves as a viscoelastic solid with elasticity dictated by particle concentration and microstructural features as represented in fractal rheo-mechanical models. Under nonlinear deformations, the crystal network yields, showing a variety of nonlinear phenomena, i.e. softening, stiffening, thixotropy. These features largely contribute to functionality or performance as essentially all processing and end-uses of fatty materials involve large nonlinear deformations. Early work on rheology of fats gave hints of their nonlinear mechanical behavior, although in many cases the measured properties were empirical. In contrast, recent efforts from our group measured fundamental rheological functions using large amplitude oscillatory shear rheology. We demonstrate the ability of this technique to discern among the bulk functionality of bakery fats (all-purpose and lamination shortenings) based on well-defined rheological signatures that also relate to the fat structure. This technique has the

potential to provide similar insights on other fatty systems and novel ideas for reformulation and

design of alternative lipid-structuring materials.

Keywords

fat, linear and nonlinear rheology, texture, structure, *trans* and saturated fatty acids

1. **Introduction**

Fats are ubiquitous in nature, foods and in many commercial applications. In our body, they serve as supply and reservoir of energy (9 kcal g^{-1}) and contribute to cellular structuring, compartmentalization, biomolecular synthesis, among other vital biological roles (Kulkarni, 2012; Marangoni et al., 2012). In foods (i.e. chocolate, butter) and other commercial products (i.e. cosmetic creams), they provide nutritional value, texture control, mouthfeel and other physical characteristics (i.e. oil binding), which play pivotal roles in consumer acceptability (Marangoni et al., 2012). From a nutritional standpoint, consumption of mono or polyunsaturated fatty acids (FA) are preferred over saturated and *trans* FAs as monounsaturated FAs are linked with reduced risk of cardiovascular disease, while the latter with higher propensity for developing cardiovascular diseases (R. P. Mensink et al., 2003; Mozaffarian et al., 2006; Uauy et al., 2009). From a mechanical perspective, texture is inherently linked to rheological properties that result from the hierarchical structure of fats (Marangoni and Narine 2002)

The complex hierarchical structures of fats, ranging in length from the molecular to the microscopic scale, are responsible for their mechanical properties (Fig. 1). At the molecular level, high-melting TAGs pack longitudinally typically in double or triple chain lengths, and laterally, following a specific subcell unit arrangement or polymorphism (α, β', β), to form the crystal lamellae (Fig. 1a) (Sato, 2001). At the nanoscale level, epitaxial stacking of 7-10 crystal lamellae give rise to plate-like structures with various surface morphologies, which are defined as the basic building blocks (Fig. 1b) (Acevedo and Marangoni 2010; Acevedo et al. 2011). At the submicron and microscopic level, crystalline nanoplatelets (CNPs) self-assemble into larger

fractal cluster or aggregates via DLA/RLA or DLCA/RLCA (Peyronel, Pink, et al., 2014) to ultimately form a volume-filling network similar to that of flocculated colloidal gels (Fig. 1c) (DeMan and Beers 1987; Narine and Marangoni 1999d). The manner in which CNPs are organized into higher-order structures can vary considerably, which in turn opens the possibility for various microstructures (i.e. spherulitic-like, needle-like, etc) embedded in a liquid oil phase (Heertje 1993; Juriaanse and Heertje 1988). These structures confer viscoelastic solid behavior ($G^{'}$>$G^{''}$) at small deformations, and their diversity reflects the adaption of fats to its mechanical function (Heertje 1993; van den Tempel 1961; Narine and Marangoni 1999d; Narine and Marangoni 1999b).

The rheological properties of fats as related to the crystal network have been a major field of study (Scott Blair 1938; Davis 1937; Blair 1954; Haighton 1959; DeMan and Beers 1987; Narine and Marangoni 1999e; Thareja 2013). Significant advances have been made in this area, enabling us to partly understand linear viscoelasticity in terms of fat microstructure (Narine and Marangoni 1999a; Narine and Marangoni 1999b; Narine and Marangoni 1999e). Of major interest, are the endeavors of Narine and Marangoni (1999b), who extended the microscopic fractal model, originally proposed for colloidal gels, to explain the elasticity of the crystal network (Narine and Marangoni 1999a; Narine and Marangoni 1999d; Coussot 2007). The fundamental basis of developed and modified fractal models is the assumption that fats self-assemble into fractal flocs or aggregates. According to this, the elastic modulus G' of the system scales in a power-law fashion with particle volume fraction $G' \sim \phi^{n}$, where n is related to the compactness of the individual clusters or mass fractal dimension (D) (Marangoni and Rousseau 1996; Narine and Marangoni 1999a; Narine and Marangoni 1999d) Depending on ϕ, G' is

dictated by the elasticity of the microstructural interlinks (weak-link regime ϕ>0.1) or that of the flocs (strong-link regime ϕ<0.1) (Narine and Marangoni 1999b; Narine and Marangoni 1999e). Despite these efforts, relating the microstructure to mechanical properties is still largely unresolved due to complexity imposed by the various structural levels. Moreover, the structure of the network "ages" over time (i.e. crystal sintering occurs) which in turn affects its mechanical properties, making the task of establishing structure-mechanical function relations a very challenging one (Scott Blair 1954).

While there has been considerable scientific interest on linear rheology at small deformations, there has been limited focus on nonlinear rheology of fats at large deformations. The study of nonlinear rheology is of outstanding fundamental and practical interest given that the morphology of the microstructure, determined by its preceding structural levels, have strong influence on the nonlinear response (Heertje, 1993). Most notably, nonlinear rheology occurs in essentially all industrial processing and end-uses of fatty materials, i.e. extrusion of shortening, spreading of butter and rubbing of a cosmetic cream. Therefore, linear rheology appears insufficient to understand the rheological function of fats. It has been recently demonstrated that multicomponent fats (shortenings) with similar linear viscoelastic properties show different nonlinear viscoelastic properties and hence diverse performance (Macias-Rodriguez and Marangoni 2016b). Likewise, it has been tacitly revealed in the literature that fats show intriguing nonlinear phenomenon including yielding, strain hardening and stress softening, thixotropic behavior, which merit special attention (Haighton 1965; Scott Blair 1938; Sone 1961; Gonzalez-Gutierrez and Scanlon 2013).

Previous works on the nonlinear rheology of fats have largely measured textural attributes by empirical methods (i.e. cone penetrometry). Conversely, nonlinear rheological characterization of colloidal gels and polymeric materials has focused on fundamental techniques including large amplitude oscillatory rheology (LAOS), which has proven extremely fruitful (Hyun et al., 2011; Petekidis, 2014).We favor the latter approach as it enables to define true material properties relating to the structure. In addition, it allows probing an ample range of deformations and timescales capturing the yielding transition of fats. This approach, powerful as it may be, needs to be used with caution to minimize potential artifacts hindering data analysis or masking small rheological differences between samples.

This reviews aims at providing an overview of the rheological properties of fats at both small and large deformations. To this end, we briefly review the hierarchical levels of organization, which range in scale from nano to micrometers and in turn determine the mechanical properties of fats. We then review linear viscoelastic properties, microscopic models relating linear viscoelasticity to the microscopic network, and place special emphasis on nonlinear viscoelastic properties as investigated by LAOS applied to fat crystal networks. Moreover, we discuss the implementation of LAOS protocol pointing out instrumental challenges associated with this technique and in general with shear rheology. Finally, we provide a study case where LAOS successfully elucidated the mechanical functionality of two contrasting type of fats: all-purpose designed to function under many bakery applications and roll-in shortening intended for lamination applications.

2. Physical length scales of fats

2.1 Molecular structure and polymorphism

Triacylglycerols molecules, made of three FA moieties esterified to a glycerol backbone, are the base constituents of fats and oil. The characteristics of the FA moieties: chain length (4-22 carbons), degree of unsaturation, isomerism, regiospecificity, determine physical properties (i.e. molecular packing, solid-to-liquid mass fractions or SFC) and pose important nutritional significance (Marangoni et al., 2012). For instance, long-linear (*trans*) saturated fatty acid chains pack more efficiently than short-kinked (*cis*) unsaturated FAs, have higher melting points and contribute to solid-like functionality (or greater SFC) (Ghotra et al., 2002). In terms of nutritional benefits, polyunsaturated fatty acids are preferred over saturated fatty acids as the primer is correlated with improved cardiovascular health, whereas *trans* fatty acids are overall not recommended as they are associated with increased risk of cardiovascular diseases (Ronald P Mensink et al., 2003; Mozaffarian et al., 2006; Uauy et al., 2009).

During nucleation, TAGs stack side-by-side in pairs following either a "chair" or "tuning fork" configuration to give rise to crystal unit cell. The unit cell is the primary unit from which the crystal lamellae is built by three-dimensional translations (Acevedo et al. 2011). The unit cell is highly asymmetric with a very long *c*-axis (relative to the small *a* and *b* short axes) whose longitude is equivalent to the thickness of the crystal lamellae as determined by long spacings in the small-angle x-ray diffraction spectra (Acevedo and Marangoni 2010; Acevedo et al. 2011). The thickness of the crystal lamellae depends on TAG packing ("back-to-back" or "seat-to-seat") which typically form double or triple chain length structures (Sato, 2001; Marangoni et al., 2012).

During crystallization, high-melting TAGs pack into a preferred polymorphic form which is defined on the basis of the subcell unit describing the lateral packing of the zigzag hydrocarbon chains ($-CH_2-$) (Marangoni et al., 2012). Three major polymorphic states with their respective subcell packing are distinguished: α (hexagonal), β' (orthorhombic), β (triclinic) (Sato and Ueno 2011). Each polymorphic form, available from the melt, evolve towards the most stable polymorphic state (β) via melt-mediated or solid-mediated monotropic phase transformations (Himawan et al. 2006). Each polymorphic form displays unique short-spacings in the Wide-angle X-ray diffraction spectra (Marangoni et al., 2012). For in-depth information on fat polymorphism, the readers are referred to the excellent reviews of Sato (Sato 2001; Sato and Ueno 2011).

2.2 Nanoscopic-to-mesoscopic structure

Early work on fat structure imaging led to long-standing assertions that micron-sized crystal aggregates were the smallest structural length scale in fats (Acevedo et al., 2011). However, further explorations on sub-mesoscale structures conclusively identified highly anisotropic crystal nanoplateles (CNPs) or crystal domains as the primary crystal units (Acevedo and Marangoni 2010; Acevedo et al. 2011). Crystalline nanoplatelets result from the epitaxial packing of typically 7-10 TAG lamellae as confirmed by TEM and SAXS experiments (Acevedo and Marangoni 2010). A large number of studies have confirmed the presence of CNPs in a wide range of binary or multicomponent lipid systems including tristearin in triolein, cocoa butter, milk fat (Marangoni and Pink 2014).

Formation and aggregation of CNPs into clusters forming the crystal network (or microstructure), is driven by Van der Waals attractions. Pioneering works based on Monte Carlo computer simulations and ultra-small-angle x-ray scattering (USAXS), have shed much-needed light in the field of fat aggregation (Peyronel, Pink, et al., 2014). These reports have elucidated the process of CNP aggregation into intermediate physical structures in the "nano-to-micro world" and the features (size, morphology) of such aggregates in binary and multicomponent TAG systems. To illustrate, for a simple binary system of tristearin (SSS) in triolein (OOO), it was reported that CNPs, characterized by a smooth surface, stacked into 1-dimensional TAGwoods (Peyronel et al., 2013). Subsequently, TAGwoods self-assembled into fractal clusters initially via diffusion limited cluster-cluster aggregation (DLCA, D = 1.7-1.8), and then via reaction-limited cluster-cluster aggregation (RLCA, D = 2.0-2.1) as steady-state relaxation is reached (Peyronel et al., 2013; Pink et al., 2013). For multicomponent systems (i.e. SSS in cottonseed oil, SSS in shea butter, SSS in partially hydrogenated canola oil) aggregation appeared far more complex as a gamut of self-assembled structures became possible (Peyronel, Quinn, et al., 2014; Quinn et al., 2014). Liquid-liquid or solid-liquid nano-phase separation induced smooth, diffuse or rough coatings on CNPs. Smooth or diffuse surfaces favored the formation of TAGwoods that either grew into larger DLCA/RLCA structures and then clusters uniformly distributed in space, or end-to-end connected TAGwoods (Peyronel, Quinn, et al., 2014; Quinn et al., 2014). Rough surfaces hindered the formation of TAGwoods, promoted a mixture of CNPs and TAGwoods or side-to-side connected TAGwoods (Peyronel, Quinn, et al., 2014; Quinn et al., 2014). In both cases, the connected TAGwood strings gave rise to a diffuse

surface. For a comprehensive description on characterization and aggregation of CNPs, the readers are referred to (Acevedo et al., 2011; Peyronel, Pink, et al., 2014).

2.3 Mesoscopic structure

Crystal aggregates form the volume-filling space network so-called the microstructure (DeMan and Beers 1987; Marangoni et al. 2012; Juriaanse and Heertje 1988; Heertje 1993; van den Tempel 1961). This level of structure is the closest to the macroscopic world and hence it has tremendous bearings on rheological properties of bulk fats (DeMan and Beers 1987; Heertje 1993; Narine and Marangoni 1999d; Tang and Marangoni 2007). It is considered the first structural level to be stressed or strained during deformation (Heertje 1993; Narine and Marangoni 1999d). The microstructure encompasses crystal aggregates differing in size (0.1 μm- 140 μm) and morphology, held by a wide spectrum of bonds of variable degree strength or reversibility (DeMan and Beers 1987; Narine and Marangoni 1999e; Shama and Sherman 1970). Some of these morphologies include broad spherulites with radially-arranged needles, closely-bound spherulites with randomly-orientated crystals, closely-bound spherical clusters and open randomly-arranged bundles (Juriaanse and Heertje 1988; Heertje 1993).Such variety in crystal morphology offers equal variety in the mechanics of deformation, i.e. the fat crystal network displays viscoelasticity, yielding, thixotropy, e.g. shear softens and subsequently restructures, local strain stiffening (van den Tempel 1961; Narine and Marangoni 1999b; Haighton 1965; Scott Blair 1954; Gonzalez-Gutierrez and Scanlon 2013; Macias-Rodriguez and Marangoni 2016b; Thareja 2013).

3. Rheological properties of fats

Rheology is primarily concerned with describing flow or deformation of matter when subjected to stress or strains deformations. Early studies on fat rheology or fat-structured materials (i.e. cheese) were undertaken as early as 1930 by the founding father of food rheology Scott Blair, and Davis (Scott Blair 1938; Davis 1937; Scott Blair 1954). These authors were the first to quantify the elastic and viscous properties of fat crystal networks, and attempted to relate fundamental linear viscoelastic measures to texture attributes (i.e. firmness, spreadability). At small or linear reversible deformations, fats behave as viscoelastic solids materials, whereas above critical or nonlinear irreversible deformations they show viscoelastoplastic behavior (Marangoni et al. 2012; Gonzalez-Gutierrez and Scanlon 2013). Linear viscoelasticity as related to the microstructural network has been vastly researched, while nonlinear viscoelasticity have been less investigated. This is unfortunate since all processing and applications of fatty materials involve nonlinear deformations, e.g. lamination of shortenings, rubbing of a cosmetic cream, that trigger nonlinear stress responses. Such responses relate intimately to performance and consumer perception and therefore merit special attention. In this section, we briefly summarize the salient points on linear viscoelasticity of fats as related to microstructure via micromechanical models. Most importantly, we cover past work on nonlinear viscoelasticity of fats and our most recent research efforts on this area. Moreover, we give general caveats for collecting shear rheology data, and investigate the rheology of complex fats: laminating *versus* all-purpose shortenings. These fat systems serve as paradigms for ductile rupture and brittle failure, respectively, and their rheological behavior is ascribed to their differing structural organization.

3.1 Linear viscoelasticity

Most of the published literature on the rheology of fats describes linear viscoelastic properties measured by small strain amplitude oscillatory shear rheology (SAOS) (van den Tempel 1961; Marangoni and Narine 2002; Narine and Marangoni 1999c; Narine and Marangoni 1999b; Rohm and Weidinger 1993; Thareja et al. 2013). During SAOS, strain inputs in the order of $\gamma_0 \approx 0.01\%$ within the linear viscoelastic region (LVR) are applied, which are typical of materials having short-range van der Waals attractions (van den Tempel 1961). Unlike polymer chains, fat crystal networks possess irreversible bonds and hence cannot be substantially strained without losing memory of their original configuration (van den Tempel 1961). Given the narrow linear envelope, rheological techniques must minimize disturbance of the underlying network. This can be achieved for example by using normal-force loading protocol for pre- crystallized fats or geometries that facilitate in-situ characterization (Macias-Rodriguez and Marangoni 2016b; Thareja et al. 2011). Under the SAOS regime, strain and stress maintain their linear proportional and the crystal network act as a viscoelastic solid ($G'>G''$) that exhibit high storage modulus ($G' \sim 10^5$-10^6 Pa) with low-frequency dependence ($G' \sim 10^5$-10^6 Pa) (van den Tempel 1961; Narine and Marangoni 1999b; Macias-Rodriguez and Marangoni 2016b; Rohm and Weidinger 1993; Thareja et al. 2013). For a sinusoidal strain excitation $\gamma(t) = \gamma_0 \sin(\omega t)$, a sinusoidal stress response is obtained and expressed as:

$$\tau(t) = \gamma_0 G'(\omega)\sin(\omega t) + \gamma_0 G''(\omega)\cos(\omega t) \quad \text{Eq. (1)}$$

In which G', the in-phase elastic or stored energy represents the real component, and G'', the out-of-phase viscous or dissipated energy represents the imaginary component of the complex modulus G^* at a given frequency (ω) (Ferry, 1980; Tschoegl, 1989; Macosko, 1994). In the LVR,

the stress $\tau(t)$ response is sinusoidal and shares the same harmonic with γ_0, shifted only by a phase angle. Material response is represented by the first or fundamental harmonic of a Fourier series. Another rheometric technique to probe linear viscoelasticity is shear creep and recovery test (Fig. 2a). This technique consists in loading and unloading step stresses for longer time scales to probe the associated relaxation phenomena (van den Tempel, 1961; Macosko, 1994). Linear viscoelasticity can be captured by a standard four-parameter Burgers model, which comprises a Maxwell model (spring and dashpot in series) coupled to a Kelvin-Voigt model (spring and dashpot in parallel) (Steffe, 1996) (Fig. 2b). In the Burgers model, the compliance function $J(t) = \gamma(t)/\tau_0$ during the creep (a) and recovery (b) is described by the following equations:

$$J(t) = \frac{t_c}{\mu_0} + \frac{1}{G_0} + \frac{1}{G_1}\left[1 - \exp\left(-\frac{t_c}{\lambda_1}\right)\right] \text{Creep Eq. (2)}$$

$$J(t) = \frac{t_c}{\mu_0} + \frac{1}{G_1}\left[1 - \exp\left(-\frac{t_c}{\lambda_1}\right)\right]\exp\left(-\frac{t_r - t_c}{\lambda_1}\right); t_r > t_c \text{ Recovery Eq. (3)}$$

Where t_c and t_r are the creep and recovery times, respectively, G_0 and μ_0 are the elastic modulus and viscosity of the Maxwell element, G_1 and μ_1 are similar parameters in the Kelvin-Voigt element and $\lambda_1 = \dfrac{\mu_1}{G_1}$ is the characteristic retardation time. Note that G_0 and G_1 are equivalent to instantaneous J_0 and retarded compliances J_1 as $J = 1/G$ in the LVR. Although incrementing the number of Kelvin-Voigt elements is necessary for describing a complex spectrum of retardation times, this increases the phenomenology of the model (Blair and Burnett 1959). From a practical

standpoint, the elastic shear modulus correlates well with textures attributes such as fat hardness and consistency (Narine and Marangoni 1999b).

3.2 Linear viscoelasticity and microscopic modelling approaches

The microstructure is critical in determining the mechanics of deformation of fats (DeMan and Beers 1987; Thareja 2013; Marangoni et al. 2012). Many rheo-physical models have been put forward ranging from the very reductionist linear chain model (van den Tempel, 1979) to the more comprehensive fractal model (Narine and Marangoni 1999b), to link the microstructure to the linear viscoelastic properties of the network (Tempel 1979; Vreeker et al. 1992; Heng et al. 2005; Tang and Marangoni 2006). The fractal model exploits the framework of fractal theory to describe the fat network as a collection of self-similar flocs or clusters that result from particle aggregation (Vreeker et al. 1992; Marangoni and Rousseau 1996; Narine and Marangoni 1999a). Above the critical volume fraction ($\phi_c \approx$ 0.05-0.10), flocs grow enough as to overlap and give rise to the elastic-like character of the network. The elasticity of system scales as a function of volume fraction (ϕ) or solid fat content (SFC/100) in two distinct regimes. These regimes include the strong-link regime and the weak-link regime (Marangoni and Rousseau 1996; Narine and Marangoni 1999a). The strong-link regime occurs at lower particle concentration (ϕ<0.1) where each individual cluster grows large, and the elasticity of the flocs rather than that of the links, dictates the elastic modulus of the system (G'):

$$G' \sim \phi^{\left[(d+x)/(d-D)\right]} \quad \text{Eq. (4)}$$

Where d is the Euclidean dimension of the embedding space (usually 3), D is the fractal dimension, which describes spatial distribution, "compactation" and morphology of the network,

x is the backbone fractal dimension (~1-1.3). It is also noteworthy that the fractal dimension provides information on the aggregation mechanism of the network, e.g. $D = 1.75$ for DLCA and $D = 2.1$ for RLCA (Narine and Marangoni 1999e). The weak-link regime occurs at higher particle concentration ($\phi > 0.1$), characteristic of most model systems and commercial fats. Here, small clusters behave as rigid or strong springs and the links among clusters or microstructures govern the elasticity of the system:

$$G' \sim \phi^{1/(d-D)} \quad \text{Eq. (5)}$$

An additional pre-exponential factor $\lambda = \dfrac{A}{\pi a d_0^2}$ may be introduced to the weak-link relationship to discern among crystal networks showing similar D and ϕ but different G' (i.e. cocoa butter and salatrim) (Narine and Marangoni 1999d). In the pre-exponential term, A corresponds to the Hamaker's constant, a to the dimension of the primary crystal unit and d_0 to the intercluster distance (Narine and Marangoni 1999b). The weak-link fractal model may be used to estimate the Young modulus ($E = \sigma/\varepsilon$) (Marangoni, 2000). Furthermore, the elasticity of some fat systems may show no power-law dependence due to stress localization in a small fraction of the network connections which serve as "weakest bonds" (Tang and Marangoni 2007). For this case, a modified fractal model accounts for separate effects of the network microstructure, stress distribution and interconnectivity as follows:

$$G' \sim \phi_e^{1/(d-D)} \quad \text{Eq. (6)}$$

Where the effective volume fraction of solids responsible for stress-bearing is $\phi_e = 1 - e^{-k\phi^b}$ and k and b are constants. For complete reviews of the network mesoscopic models, the readers are referred to Narine and Marangoni (1999d), and Tang and Marangoni (2006).

3.3 Nonlinear viscoelasticity

Under increasing deformations, interlink bonds start to break, triggering yielding of the crystal network which switches gradually from solid-like to liquid-like behavior (Marangoni and Rogers 2003). Yielding as related to strain and stress, is dependent on solid volume fraction, particle size, fractal dimension of the network, among other parameters (Marangoni and Rogers 2003). Despite of much debate about the existence of a "true" yield stress, the yield stress remains a valuable parameter in the rheological characterization of fats and other pasty materials (Coussot, 2007). As yielding takes place, fats display rich nonlinear viscoelastic responses (i.e., network softening and structural reversibility) which shall be investigated in depth, as these features pose enormous relevance in the usability of fats (Blair 1954; Thareja 2013; Sone 1961; Macias-Rodriguez and Marangoni 2016b). A survey of the literature reveals that most of the published work on nonlinear viscoelasticity involves more empirical methods that measure texture attributes than fewer fundamental methods that characterize true material properties. In what follows, we describe both types of approaches and place special emphasis on large amplitude oscillatory shear (LAOS) rheology as a novel and emerging technique to measure nonlinear viscoelasticity of fat crystal networks.

3.3.1 Empirical methods

Major empirical methods include indentation or penetration tests that assess viscoelastic texture attributes such as hardness or firmness, "yield" value and spreadability of butter, margarine, shortenings and other fatty products (Blair 1954; Haighton 1959; DeMan and Beers 1987). Falling rods or balls measured hardness of butter and margarine as correlated to their temperature and melting (Scott Blair, 1954). Penetration with standard cones includes the official method of the American Oil Chemists' Society (AOCS Cc 16-60) to evaluate fat texture, which deserves special attention (Haighton, 1965). This method employs constant load or constant speed cone geometries with variable or no truncation, to penetrate a fat sample. Depending on the specifics of the test, several empirical relationships have been developed to calculate textural attributes. For example, hardness index $HI = W/p$ and "yield value" $C = KW/p^n$, where W is the cone weight, p is the penetration depth, K is a cone constant dependent on angle, and n is an arbitrary material constant equal to 1.6 for margarine, butter and shortenings (Haighton 1959; deMan et al. 1989; deMan, et al. 1991; Shen, et al. 1991; Hayakawa and deMan 1982). The intended use of shortenings and margarines can be differentiated based on these parameters, although that is not always necessarily the case (Haighton 1959; Macias-Rodriguez and Marangoni 2016a).

Despite the economy and simplicity of this method, several considerations should be borne in prior to using the cone penetrometer. For instance, whether hardness is measured remains debatable, considering the definition of 'hardness' as "the resistance of the surface of a body to penetration." In the same manner, the concept of "yield value" is ill-defined and possibly, it is far from the true yield stress by several orders of magnitudes, considering the intuitively larger shear deformations associated specially with "pointy" or small-angle cones (Atkins and Tabor 1965). Our reservations to this method are justified by previous correlations of cone penetrometer

parameters with spreadability of butter and margarine, a property involving extensive shear deformations and structural breakdown (Haighton 1959; Haighton 1965; Shama and Sherman 1970).

Some other methods to determine hardness and spreadability include the Mohr and Wellm's cone- and sphere- yield tests, Trouton measure of sagging of a beam fastened at its ends, uniaxial compression and imitative tests (Texture Profile Analysis: TPA) (Scott Blair, 1954; Szczesniak, 2002). Previous studies have shown that the hardness obtained from compression does not necessarily correlate with that from cone penetrometry. Finally, one of the most subjective methods is the so-called "thumb" test that relies on the capability in discriminating textural properties such as firmness, recovery and plasticity of fats by purely tactile sensitivity (Cavillot et al., 2009; Garcia-Macias et al., 2011, 2012; Pajin et al., 2011).

3.3.2 Fundamental methods

Much of the fundamental work in fat rheology involves capillary flow, creep and recovery tests, uniaxial compression, steady-shear tests, oscillating viscometry and parallel-plate plastometry, steady-shear tests. Capillary tests measure steady shear viscosities and closely resemble manufacturing processes of soft solids, i.e. pipe flow, paste-ram or cold extrusion (Macosko, 1994; Castro et al., 2010). A capillary rheometer uses gravity, compressed gas or driving tools such as a piston ram to exert pressure and force the material through a barrel and die with diameters D_0 and D, respectively (Macosko, 1994). During this operation, pressure drops are recorded, and used along with the flow rate of the tube to determine steady shear viscosities. Previous reports showed that thin fat layers and hardened peanut oil flowing through capillaries

display either simple or anomalous nonlinear behavior, i.e. (Scott Blair, 1954). True fluids hold

linear relationship between shear stress *PR/2L* and shear rate $4V/\pi R^3$ at the wall when flowing

through a capillary with radius *R* and length *L* under pressure *P*. It was found that the most

hardened peanut oil mixtures behave as Bingham plastic fluids, obeying the *Buckingham-Reiner*

expression, $V = \dfrac{\mu \pi R^4}{8L}\left(P - \dfrac{4}{3}p + \dfrac{p^4}{3P^3}\right)$, where μ corresponds to the linear slope of the curve and

p to the yield value below which there is a plug flow (Scott Blair, 1954).

Creep and recovery tests for standardized times, stress loads or deformation loads showed that

butter and margarine has elastic recoverable and plastic non-recoverable components from which

elastic moduli and viscosity were determined. Successive experiments with increased stresses

suggested a type of stress softening (fall in viscosity) in butter, whereas experiments with

increased strains pointed out to a type of strain-hardening (rise in viscosity) in butter and 25%

glyceryl tristearate in oil (Blair 1954; van den Tempel 1958). Experiments on the effects of

work-softening, loading creep phase and temperature revealed that butter recovered more of its

instantaneous elasticity and less of its Newtonian viscosity during aging compared to margarine.

This was apparently due to higher shear sensitivity of margarine given a larger proportion of

irreversible bonds originally present in the network (Shama and Sherman 1970). Increased stress

and loading time decreased more the instantaneous elasticity than the retarded elasticity and

viscosity, whereas increased temperature strongly diminished all viscoelastic parameters (deMan

et al. 1985). Uniaxial compression tests revealed similar strain-hardening at rising true strains $\varepsilon =$

4%, followed by strain-softening and ideal plastic response at larger deformations (Gonzalez-

Gutierrez and Scanlon 2013).

Steady shear experiments demonstrated that margarines failed to follow the so-called Cox-Merz "rule" that implicates correspondence between steady state viscosity η and complex viscosity η^* (Bistany and Kokini 1983). However, evidence of slip, edge fracture, transients and thixotropic effects affecting the reproducibility of the test and the steady state data were not ascertained in this report. Oscillating viscometry and parallel plate plastometry indicated thixotropic behavior of butter and margarine as measured by the decrease of viscosity, elasticity and yield value after kneading and their subsequent recovery after prolonged setting time. Rupture and recovery were attributed to crystal melting and recrystallization of the network (Sone, 1961).

Although some of the abovementioned methods, both empirical and fundamental, provide useful information on the nonlinear viscoelasticity of fats, they have many inherent limitations. For example, uniaxial compression allows only calculation of apparent elastic modulus and viscosity. Moreover, the elastic modulus cannot be precisely determined below 2% as is the case for most fat systems, while the viscosity is subject to large errors after yielding (Kloek et al. 2005; Gonzalez-Gutierrez and Scanlon 2013). Shear creep or stress relaxation impose sudden and large displacements providing inhomogeneous and uncontrolled flow. Steady shear gives an indication of shear-sensitivity, formability or shaping of fat during processing, nevertheless; fats may slip at the shear-rates imposed by these tests. Likewise, empirical test such as cone penetrometry, useful for drawing correlations at best, suffer from lacking a sound theoretical foundation and do not measure clearly defined physical properties. Therefore, there is an obvious need to adapt novel rheological techniques that provide true criteria relatable to the macroscopic functionality of fats during nonlinear deformations.

To address this gap, recent work in our laboratory has explored the use of large amplitude oscillatory shear (LAOS). Lately, there has been growing scientific interest on LAOS which has proven extremely useful, to understand mechanical functionality of a variety of polymeric, colloidal and biological materials, indistinguishable by SAOS (Ewoldt et al., 2007; Hyun et al., 2011; Petekidis, 2014). Fig. 3 provides a striking example of the shortcomings of the traditional SAOS test, and motivation for adapting the LAOS protocol. While the viscoelastic moduli G_1' and G_1'' remain unremarkable in the LVR, these material functions depart drastically outside the LVR, e.g. G'_1 and G''_1 shows a steady decrease for laminating shortening, whereas G'_1 and G''_1 display abrupt drop and backward bending for all-purpose shortening, evoking strong softening and catastrophic failure for the latter. These features are also captured in the strain-stress plots, e.g. the local slope, reflecting the stress increase per increment of applied strain, appears steeper for an all-purpose than for a laminating shortening. Likewise, an all-purpose shortening shows a strong peak overshoot ensued by marked decay of stress, whereas a laminating shortening exhibits a stress plateau. Similar behavior has been previously reported in compression and imitative large deformation tests where a fat is deemed plastic if the required stresses at low amplitudes and large amplitudes are comparable, and a fat is regarded work-softened if the required stress at low amplitudes is higher than that of at large amplitudes (Heertje, 1993; de Bruijne and Bot, 1999). Currently, a protocol for easily characterizing fat materials with this type of behavior lacks.

Large amplitude oscillatory shear rheology offers many advantages over traditional methods including simultaneous viscoelastic characterization in both deformation and timescale domains, controlled flow, ample operational window, superior sensitivity and several frameworks for data

interpretation (Hyun et al., 2011). LAOS enables varying two parameters independently: the amplitude of the deformation γ_0 and frequency ω of deformation, rendering a two-dimensional regime map-space known as the Pipkin space (Pipkin, 1972). The Pipkin space relates viscoelastic responses as a function of loading amplitudes, shear rates and timescales of relaxation (Pipkin, 1972). It also seamlessly connects nonlinear viscoelastic measures $G'(\omega, \gamma_0)$ and $G''(\omega, \gamma_0)$ with linear viscoelastic moduli $G'(\omega)$ and $G''(\omega)$, and with the steady flow viscosity $\eta(\dot{\gamma})$ (Dealy and Wissbrun 1999; Ewoldt and Bharadwaj 2013). LAOS generates relatively controlled flow allowing for probing weakly-bonded and stiff materials such as high-volume fraction fats that fracture, slip, and migrate out of the gap during steady shear (Hyun et al., 2011). It provides a wider deformation window due to improved resolution as deformation inputs are extended to medium and high amplitudes. Hence, LAOS is able to discriminate among structural architectures, which are insensitive to SAOS (Hyun et al., 2011). This is particularly advantageous for fats due to their restricted linear envelope. Substantial improvement on the signal-to-noise ratio, two to three orders of magnitude higher than former work on polymer rheology (S/N $\approx 10^2$), has been achieved due to improvements in state-of-the-art hardware and software (i.e. more sensitive torque transducers, oversampling techniques, accessible computational power and special FT algorithms) (Hyun et al., 2011). Likewise, a wide variety of frameworks have been proposed to quantify the nonlinear viscoelastic response including Lissajous-Bowditch curves, Fourier Transform (FT), stress-Chebyshev decomposition method, power-function expansions, time-dependent moduli, among others (Wilhelm 2002; Ewoldt et al. 2008; Rogers et al. 2011; Rogers 2012).

3.3.2.1 LAOS fundamentals

At large amplitudes (LAOS), complex and nonlinear shear stress responses arise in many viscoelastic materials including fats. For a strain input test, the stress material response is considered nonlinear when either of the viscoelastic moduli are variant to changes in γ_0, e.g. $G'(\omega, \gamma_0)$ or $G''(\omega, \gamma_0)$ or when the response is not longer sinusoidal. As a result, G' and G'' lose their mathematical and physical underpinnings in this region (Hyun et al. 2011; Ewoldt et al. 2008).

3.3.2.2 Nonlinear stress waveforms

Nonlinear sinusoidal waveforms represent the most simple way to qualitative detect and interpret nonlinear data. They may be presented in the form of time-domain signals $\tau(t)$ or in two-coordinate axes figures referred as to Lissajous-Bowditch curves. Lissajous-Bowditch curves are orbital trajectories of γ_0 on the abscissa and $\tau(t)$ on the ordinate (elastic representation) or $\dot{\gamma}_0$ on the abscissa and $\tau(t)$ on the ordinate (viscous representation). As an illustration, Fig. 4 shows the stress response in the time domain and elastic and viscous perspectives of the Lissajous-Bowditch curves within the LVR and outside the LVR for a commercial shortening. In the LVR region ($\gamma_0 = 0.01\%$), the shape of the stress remains as a perfect sinusoid, whereas the Lissajous-Bowditch plots appear as ellipsoids where the tangent slope corresponds to G' and the area enclosed by the ellipsoid represents G''. Outside the LVR, the stress signal becomes distorted leading to non-ellipsoidal rectangular Lissajous-Bowditch curves that enclose larger areas (Ewoldt et al., 2008; Hyun et al., 2011). With the aid of the Lissajous-Bowditch curves, typical

features, i.e. global strain softening of the network, and additional features obscured by the average viscoelastic moduli, i.e. local strain stiffening, are revealed. Global or average elastic softening, is manifested as the intercycle clockwise rotation in slope of the stress-strain curve at strain minima $\gamma_0 = 0$ (where strain rate   is at maxima) toward the strain-axis. Local strain stiffening is clearly visible as the intracycle upturn of the shear stress at strain maxima $\gamma_0 = \max$ (where $= 0$). Stress overshoots, akin to those generated during steady shear flow, indicate substantial disruption of the microstructure. The reversibility of the stress overshoot within the period of oscillation evokes microstructure "healing" or thixotropy (Renou et al. 2010; Kim et al. 2014; Ewoldt and McKinley 2009) as previously reported for margarines and commercial shortenings (Sone 1961; Macias-Rodriguez and Marangoni 2016b)

3.3.2.3 Fourier transform (FT) rheology

Although Lissajous-Bowdtich curves provide a physical picture of nonlinear viscoelastic responses, they do not provide any quantitative parameter describe such responses. Fourier transform (FT) rheology constitutes the foremost method for quantifying nonlinear responses (Wilhelm 2002). In FT rheology, the time-varying stress signal is expressed in a frequency-domain Fourier space encoding components that are in-phase and out-of-phase with the strain input (Dealy and Wissbrun 1999; Giacomin and Dealy 1993). For a sinusoidal strain input $\gamma(t) = \gamma_0 \sin(\omega t)$, the Fourier series of the stress response is represented as follows:

$$\tau(t) = \gamma_0 \sum_{\substack{n=1 \\ n\,odd}}^{\infty} \left[G_n^{'}(\omega, \gamma_0) \sin(n\omega t) + G''_n(, \gamma_0) \cos(n\omega t) \right] \text{ Eq. (7)}$$

Where n captures higher-order harmonics in the expansion which equals an integer number of the excitation or fundamental frequency in the nonlinear regime and reduces to $n = 1$ in the linear region (Fig. 4 $\gamma_0 = 0.01\%$), with its corresponding real and imaginary coefficients represented by the generalized storage and loss modulus G_n' and G_n'' ($n = 1, 2, 3\ldots$), respectively (Wilhelm, 2002). Higher-order harmonics are typically odd due to non-negativity of the stored energy although even harmonics may appear in the signal due to broken shear symmetry e.g., with responses that have not yet reached the time-periodic state (Christensen 1982; Ewoldt and Bharadwaj 2013). To quantify the nonlinear viscoelastic response, normalized intensities of the leading-order 3rd harmonic ($I_{3/1}$) or total Harmonic Distortion are typically used in combination with first-harmonic moduli as reported by the rheometer (G_1', G_1''). The use of the first-harmonic moduli is arbitrary although it provides some meaningful information (Hyun et al. 2011; Ewoldt et al. 2008). Depending on the strain-dependence of G_1' and G_1'', nonlinear response of complex materials is classified into four groups: type I, strain thinning (G_1' and G_1'' decreasing); type II, strain hardening (G_1' and G_1'' increasing); type III, weak strain overshoot (G_1' decreasing, G_1'' increasing followed by decreasing); type IV, strong strain overshoot (G_1' and G_1'' increasing followed by decreasing) (Hyun et al., 2002). It has been observed that fats yield without and with weak or strong local maxima, that is fats show type I, type III and type IV behavior depending on their formulation and processing regimes (Macias-Rodriguez and Marangoni 2016b).

3.3.2.4 Chebyshev decomposition method

Although FT-rheology spectra offers a simple and mathematically-robust method for characterizing material nonlinearities, higher harmonics do not lend any physical insight. In the

last decade, there has been significant progress in the development of mathematically- and physically- sound frameworks for analyzing LAOS responses such as the Chebyshev stress-decomposition method and the time-dependent moduli to measure a sequence of physical processes, being the former one of the most generalized methods (Ewoldt et al. 2008; Rogers 2012). In the following theoretical description of the Chebyshev stress-decomposition method for LAOStrain protocol, we refer to the pioneering works of Cho et al. (2005); Ewoldt et al. (2008) and (Ewoldt and Bharadwaj, 2013). The Chebyshev stress-decomposition extends the so-called geometrical interpretation method originally introduced by Cho et al. (2005). The Chebyshev stress-decomposition overcomes two major shortcomings of this work. First, it provides a unique description of the decomposed stress signal by mutually-orthogonal first-order Chebyshev polynomials. Second, it defines unequivocal material parameters for quantifying nonlinear viscoelasticity, which reduce to the conventional linear viscoelastic moduli in the LVR (Ewoldt et al. 2008). In brief, the total stress response is expressed as the sum of the elastic τ'(x), where $x = \gamma / \gamma_0 = \sin \omega t$ and viscous stresses τ'' (y), where $y = \dot{\gamma} / \dot{\gamma}_0$, based on the idea that τ' and τ'' are odd functions of x and y, respectively. Unlike the closed loops observed in the Lissajous-Bowditch projections, the decomposition of the total stress renders single-valued functions of strain and strain-rate, respectively, and relates to the Fourier series as follows:

$$\tau' \equiv \frac{\tau(\gamma,\dot{\gamma}) - \tau(-\gamma,\dot{\gamma})}{2} = \gamma_0 \sum_{n:odd} G_n'(\omega,\gamma_0)\sin n\omega t \quad \text{Eq. (8)}$$

$$\tau'' \equiv \frac{\tau(\gamma,\dot{\gamma}) - \tau(\gamma,-\dot{\gamma})}{2} = \gamma_0 \sum_{n:odd} G_n''(\omega,\gamma_0)\cos n\omega t \quad \text{Eq. (9)}$$

The elastic and viscous stress components can then be described unambiguously by orthogonally-integrable Chebyshev polynomials of the first kind over the finite domain [-1, +1] as:

$$\sigma'(x) = \gamma_0 \sum_{n:odd} e_n(\omega, \gamma_0) T_n(x) \quad \text{Eq. (10)}$$

$$\sigma''(y) = \dot{\gamma}_0 \sum_{n:odd} \upsilon_n(\omega, \gamma_0) T_n(y) \quad \text{Eq. (11)}$$

Where $T_n(x)$ and $T_n(y)$ correspond to nth-order of the Chebyshev basis functions, γ_0 and $\dot{\gamma}_0$ represent the maximum in-cycle strain and shear rate, and $e_n(\omega, \gamma_0)$ and $v_n(\omega,\gamma_0)$ refer to the elastic and viscous odd Chebyshev coefficients of order n. The generic form of the Chebyshev polynomials of the first kind is given by $T_{n+1}(x) = 2xT_n(x) - T_{n-1}(x)$. The Chebyshev coefficients are directly related to the higher order Fourier coefficients in the time-domain as: $e^n = G'_n(-1)^{(n-1)/2}$ and $v^n = G''_n / \omega = \eta'_n$, respectively. Just as the third-order Fourier harmonic, the third-order Chebyshev basis function hints the onset of nonlinearity in addition to assign physical meaning to the nonlinear stress signal. Material functions G'_1 and G''_1 denote average or global stress responses equivalent to first-order Chebyshev coefficients as $e_1 \rightarrow G_1'$ and $v_1 \rightarrow \eta' = G''_1/\omega$ in the LVR given that effective higher-order contributions tend to zero. When higher-order Chebyshev coefficients become significant, the elastic and viscous stresses set along the strain and strain-rate axis respectively, changing gradually to non straight lines (e.g., bend upward or local strain stiffening or bend downward or local shear thinning). Ewoldt and Bharadwaj (2013), recently demonstrated that the signs of the leading-order third Chebyshev coefficients reveal the

input function: strain or rate-of-strain, that drives the average elastic and viscous stress responses. These interpretations are valid as long as the third-order harmonic define the curvature of the local concavities (or bends as previously called). For example, for fats, negative-average elasticity ($e_1 < 0$), and negative average viscosity ($v_1 < 0$) coupled with positive intracycle elasticity (or local strain stiffening) ($e_3 > 0$) and negative intracycle viscosity (or local strain-rate thinning) ($v_3 < 0$), indicate that global elastic softening and global viscous thinning responses are driven by large instantaneous rates-of-strain, respectively.

To capture local elastic- and viscous- effects at minimum- and large- instantaneous strains or rates-of-deformation, the following meaningful nonlinear metrics have been proposed by Ewoldt et al. (2008):

$$G_M^{'} \equiv \frac{d\tau}{d\gamma} = \sum_{n:odd} nG_n^{'} = e_1 - 3e_3 + \ldots, \ \text{Eq. (12)}$$

$$G_L^{'} \equiv \frac{\tau}{\gamma} = \sum_{n:odd} G_n^{'}(-1)^{(n-1)/2} = e_1 + e_3 + \ldots, \ \text{Eq. (13)}$$

$$\eta_M^{'} \equiv \frac{d\tau}{d\dot{\gamma}} = \frac{1}{\omega}\sum_{n:odd} nG_n^{''}(-1)^{\frac{n-1}{2}} = v_1 - 3e_3 + \ldots, \ \text{Eq. (14)}$$

$$\eta_L^{'} \equiv \frac{\tau}{\dot{\gamma}} = \frac{1}{\omega}\sum_{n:odd} G_n^{''} = v_1 + v_3 + \ldots, \ \text{Eq. (15)}$$

Where $G_M^{'}$ is the minimum-strain or tangent modulus at $\gamma_0 = 0$ and and $G_L^{'}$ is the large-strain or secant modulus at $\gamma_0 = \gamma_{max}$. Likewise, $_M^{'}$ is the minimum-rate viscosity and $_L^{'}$ is the large-rate viscosity. These deliberately-chosen material functions reduce to G'_1 and G''_1 ($\eta' = G''_1/\omega$) in the

linear regime. A graphical depiction of these measures in the elastic and viscous Lissajous-Bowditch projections is shown in Fig. 5. Alternatively, relative differences between local elasticities and local dynamic viscosities at large- strain or shear-rates and at minimum strains or shear-rates are captured by adimensional strain stiffening $S \equiv \dfrac{G_L^{'} - G_M^{'}}{G_L^{'}}$ and shear thickening

$T \equiv \dfrac{\eta_L^{'} - \eta_M^{'}}{\eta_L^{'}}$ ratios. For simple linear viscoelastic responses, $S,\ T = 0$. For nonlinear responses, $S,\ T > 0$ indicates intracycle- strain stiffening and shear-thickening and $S,\ T < 0$ corresponds to intracycle- strain softening and shear-thinning. Analogous nonlinear rheological material functions have been described for a LAOStress protocol (Dimitriou et al., 2013).

4. LAOS Data collection

Several experimental considerations shall be borne in mind when performing LAOS experiments including the data collection method, the type of experiment, e.g. strain control versus stress-control tests, and potential challenges arising during shear experiments. LAOS requires the collection of raw oscillatory waveforms which is typically achieved by two ways. The first involves collecting strain stress signals using standard capabilities included in commercial rheometers software (i.e., *TA Orchestrator* software, *Raw data LAOS* waveform) (Ewoldt et al. 2008; Läuger and Stettin 2010). The second consists in installing additional hardware that allows collection and conversion of analog voltage outputs of torque and motor displacements into digital signals using an analog-to-digital converter (ADC) card (Wilhelm, 2002). Although the latter approach confers superior sensitivity, we favor the former as it provides adequate sampling

rates, signal-to-noise ratios, and does not require extra instrumental setup as highlighted by Ewoldt et al. (2008).

The selection between strain- and stress- controlled protocols is influenced by three main factors (Ewoldt, 2013). First, the rheometer design constrains performance and sensitivity under stress or strain control mode. Second, the processing application supports the type of test. Third, the framework used for data reduction, analysis, and the application of structure-rheology models to the data (when applicable) determine the type of test. Considering these factors, we opted to use LAOStrain experiments for investigating the rheological behavior of fats in lamination-like conditions. Moreover, slight increments in the stress input (LAOStress) would lead to substantial jumps in strain deformation, given the shear-sensitivity of the fat microstructure (Läuger and Stettin 2010). During rolling, fat is also subject to drag flows depending on the speed (or frequency) of the rotating cylinders, deformations which can be mimicked using LAOStrain. The use of LAOStrain experiments make it also possible to analyze our data by the well-developed Chebyshev stress decomposition method (Ewoldt et al. 2008).

5. Experimental difficulties in shear rheology

Rheological experiments can be plagued by several artifacts that obscure differences on mechanical behavior of materials or inform false mechanical behavior at worst. Therefore, it is necessary to offer a basic overview of technical difficulties encountered in shear rheology and provide diagnosis and remedies to some of these "bad symptoms." It is our purpose to raise awareness among practitioners of these issues, so they consider them when conducting rheology of fatty materials. For a comprehensive description on these and other experimental challenges,

the reader is referred to the excellent treatise of Ewoldt et al. (2015), from which this section is built upon. Experimental issues include but are not limited to: instrumental inertial, slip at boundaries, gap setting and gap underfilling, edge fracture and other intrinsic nonlinearities attributed to the measuring geometry or instrument (Ewoldt et al. 2015).

Rheometric inertia occurs due to unsteady motion at the moving boundary where both load and displacements are simultaneously measured, which is the case for most rheometers. Instrument leads to measured torque (T) signal associated not only with material deformation but also with instrument acceleration during unsteady motion. This effect may be neglected as long as $T_{material} > T_{inertia}$ (typically the case of most fat systems), but in any case may be diagnosed by checking the raw phase ($0° < \delta < 90°$) at high frequencies, or identifying damping oscillations within short-time creep responses from which the viscoelastic moduli can be calculated (Ewoldt et al. 2015). Slip is a prevalent artifact largely overlooked in the rheological characterization of fat-based materials. It is plausible that the self-lubricated nature of fats prevent them from sticking firmly to the contacting boundaries. Key symptoms of slip include gap-dependence of apparent stress and shear-rate, reduced flow stress, and if present strongly, it can be visually observed as "free" motion of the contacting surfaces or migration of the sample outside the measuring gap (Ewoldt et al. 2015; Zhong and Wang 2003). Fig. 6 depicts the effect of slip in the rheology of a water-in-oil emulsion (Nivea Lotion) and a cake shortening during steady shear and LAOS tests, respectively. For the first case (Fig. 6a), the data that superposes for all gaps for roughened plates confirms the absence of slip, while the data that shifts to higher apparent strain rates for increasing gaps for smooth plates lends evidence of slip (Ewoldt et al. 2015). For the second case (Fig. 6b), the data that display an increase followed by a decrease of intracycle or

local strain-stiffening, as measured by $(G'_L - G'_M)/G'_L$, indicate absence of slip, whereas the data that show inconsistent strain-stiffening behavior signals to wall slip. Some of the approaches to check for and minimize slip include collect data at different gaps, modifying measuring geometries, assessing sample adhesion to different contacting boundaries such as sandpaper (the most typical), crosshatched plates, filter paper (like in our example), grooves or "cleats" (Ewoldt et al. 2015; Macosko 1994; Castro et al. 2010).

Errors due to gap setting, edge fracture, gap under- filling are equally important during shear rheological characterization. For smaller gaps, apparent viscosity may decrease due to gap offset between the calibrated gap (smaller) and the true gap. For larger gaps, the offset condition may be mitigated if smaller radius plates are used although this comes to the expense of lower-torque boundary. For larger gap, there is also higher probability of edge failure (i.e. migration outside gap, edge fracture) and heterogeneous deformation (i.e. plastic deformation) especially for viscoelastic materials and pasty materials such as fats during nonlinear tests. Edge fracture is particularly relevant to stiff fats (i.e. cocoa butter, shortenings) and can be detected by visually monitoring the edge of the sample and noticing the reduction of the apparent stress due to decrease of effective contact area or gap dependence of the data (Zhong and Wang 2003). Overall, edge effects seriously limit the strain amplitude or stress amplitude window. Regarding gap setting, it is recommended that D/h (Diameter/gap height) be in the range of 10-50. Sample overfilling or underfilling greatly affect the measured torque as dependent on radial contact $T \sim (1/R^3)$ of the samples with the plate boundaries (Macosko, 1994). Underfilling due to contraction may arise during formation of the volume-filling network of fats, or sol-to-gel transition of organogels. It can be evidenced as the development of a large negative normal force

and leads to erroneous estimation of network elasticity G'. Viable ways to eliminate this issue include applying zero normal force control during crystallization or using internal gap adjustment procedures to compensate for sample contraction (Mao et al. 2016; Läuger and Stettin 2010; Morales-Rueda et al. 2009).

Finally, geometry configurations, intrinsic system nonlinearities and transients affect the reproducibility of rheometric data. Certain geometries such as parallel plate significantly weakens the relative intensity of the higher harmonic components or simply introduces qualitative artifacts (Ewoldt et al. 2010; Giacomin et al. 2015). These effects are attributed to the non-affine deformation field inherent to plate-plate geometry as typically only the sample located at the periphery experiences the highest shear-rate amplitude (Macosko, 1994). Likewise, instrumental features such as active deformation control loops and temperature control units (e.g., peltier versus forced-convection oven) can introduce additional nonlinearities (e.g., higher or lower $I_{3/1}$ due to different thermal conditioning) (Merger and Wilhelm 2014). Finally, non-equilibrium transients effects hinder the application of the LAOS protocol. Some solutions to these issues involve comparing the results obtained from homogenous (e.g., cone-plate) and heterogeneous (e.g., plate-plate) kinematics side-by-side, awaiting sufficient time for thermal equilibration and for decay of transients. For the latter, the moduli can be monitored as a function of time or number of oscillatory cycles. Overlapping and symmetry of the Lissajous-Bowditch curves provide good indication of absence of preferential flow and attainment of steady state (Li et al. 2009).

6. Structure and mechanical function of fats: a case study

Here we present a case study where rheometric techniques (especially LAOS) are exploited to discriminate between two classes of rheologically complex fats: roll-in and all-purpose shortenings, and establish function-structure relationships in these materials. The approach used herein is applicable to many other classes of lipid-based materials where functionality and rheology are inherently related.

A roll-in or laminating shortening is a highly functional tough material (strong and ductile) used in the manufacture of croissants, Danish and puff pastry and other such laminates. Roll-in shortening standas out from any other fat since they can be extruded, squeezed and shaped into micron-width films without breaking or losing their deformation. During manufacture of pastries, roll-in shortenings are exposed to strong shear and extensional flows involving rates of deformation of 1-100 s^{-1} and pressures of up to 50kPa (Steffe, 1996). The use of roll-in shortenings in laminated baked goods render crucial processing characteristics such as uniform sheeting and lamination, optimal bubble formation and lift that result in good sensory attributes such as flakiness and good mouthfeel (Ooms et al., 2015). On the other hand, an all-purpose shortening is used for multiple bakery applications primarily cake and icing and might be even used for the manufacture of laminates. However, it is a fact that an all-purpose shortening does not perform as good as a laminating shortening (Fine et al., 2006). The functionality of a laminating shortening has long been explained using physicochemical arguments. "Optimal" physicochemical properties have been outlined for this product: ϕ = 0.25-0.20 at 20-30°C, T_{melting}>40°C, β' polymorphism and high "yield value" as determined by cone penetrometry (Ooms et al., 2015). Nevertheless, we have conclusively demonstrated that laminating shortening can share similar physicochemical properties with other bakery fats (Macias-Rodriguez and

Marangoni 2016a). We have shown that rather the rheology of these materials related to structure, play an essential role in functionality. A further motivation for studying laminating shortenings stems not only from their unique rheological function but also from the fact that these materials are rich in "hard fat" content (30% by weight of combined *trans* and saturated fatty acids).

To mimic elongational and shear flows during rolling, oscillatory shear experiments sweeping from small (SAOS) to large (LAOS) amplitudes at $\omega = 0.1\text{-}5.9$ rads^{-1}, and capillary rheology were conducted. At a fixed frequency $\omega = 3.6$ rads^{-1}, similar linear viscoelasticity and strikingly different nonlinear viscoelasticity were observed as earlier mentioned, e.g. laminating shortening behaves as a ductile viscoelastic solid, whereas all-purpose shortening act as a brittle viscoelastic solid. This behavior is in line with the macroscopic appearance of the samples during capillary rheology and compression tests. During extrusion, a laminating shortening has the ability to be drawn into continuous fine "threads" (Fig. 7a, c), ~1mm of diameter, without fracturing, whereas an all-purpose shortening forms into thicker, less uniform filaments that break easily and support less elongation (Fig. 7b). During compression, e.g. the surface of a laminating shortening (Fig. 7d) is free of cracks (or at least cracks are invisible within the length scale of observation), while the surface of all-purpose shortening (Fig. 7) is full of cracks.

To investigate the yielding process and pinpoint differences in material mechanical functionality, we interrogate the LAOS response by using a number of analysis techniques including FT rheology, Lissajous-Bowditch curves and Chebyshev-stress decomposition. All shortenings show similar quantitative and qualitative behavior depending on their functionality (Macias-Rodriguez

et al., 2017). FT coefficients and material functions determined from stress-decomposition via Chebyshev analysis are reported at a fixed frequency $\omega = 3.6$ rads^{-1} (Fig 9). Regarding Fourier coefficients, the leading-order harmonic $I_{3/1}$ (Fig. 9) rises above ~5% at $\gamma_0 \geq 0.05$, which signals the boundary between linear and nonlinear region and coincides with the mild distortion of the Lissajous waveforms in both samples (Fig. 8). Subsequently, $I_{3/1}$ increases exponentially as a function of strain input and stabilizes to a plateau at $\gamma_0 \approx 10\%$. It is observed that the peak intensity of $I_{3/1}$ is roughly twice higher for an all-purpose shortening than for a roll-in shortening, revealing that a roll-in shortening undergoes a more delayed transition toward the non-linear regime (Fig. 9) (Macias-Rodriguez and Marangoni 2016b).

Elastic and viscous Lissajous-Bowditch curves are depicted in the two-dimensional$\{\omega, \gamma_0\}$ Pipkin (Pipkin, 1972) regime maps (Fig. 9). Throughout the frequency range, at $\gamma_0 < 0.09\%$ (not shown), linear viscoelastic responses dictate the stress signal as correlated with ellipsoidal Lissajous-Bowditch curves and linear decomposed elastic and viscous stresses (dotted lines). At $\gamma_0 \geq 0.09\%$, nonlinear viscoelasticity initiate, indicated by nonelliptical curves caused by periodic variations in the total stress. As the strain amplitude keeps increasing, roll-in and all-purpose shortenings display rich nonlinear response in which the elastic Lissajous-Bowditch curves shows stress upturns indicating local strain stiffening for $\gamma_0 \geq 0.57\%$. This is concomitant with the appearance of stress bends at   invoking viscous shear thinning. The nonlinearity is sufficiently large as to induce self-intersection and formation of secondary loops $\{\omega = 3.6, 6$ rads^{-1}, $\gamma_0 \geq 6\%\}$, physically related to a material that accumulates new deformations slower than it unloads instantaneous elastic stresses (Ewoldt et al. 2008), and showing strong overshoots such

as an all-purpose shortening (Fig. 3). At sufficiently high strains ($\gamma_0 \geq 6\%$), Lissajous-Bowditch curves become increasingly rectangular and larger indicating marked plastic response as more evident in a roll-in shortening. Based on the Lissajous-Bowditch curves, it can be inferred that a laminating shortening presents less degree of softening and thinning than an all-purpose shortening, nevertheless; we shall determine nonlinear metrics that support these observations

Intracycles elastic and viscous material functions are shown in (Fig. 10). We observe marginal differences in the ratio between large- (G_M') and small- (G_L') strain elastic moduli (Fig. 10a) given that fats do not display high elasticity. In contrast, η_M' and η_L' differ considerably as a function of γ_0, i.e., the normalized minimum- and maximum- shear rate viscosities of a roll-in shortening were over two times higher than those of an all-purpose shortenings. Therefore, it is concluded that a roll-in shortening experiences substantially more viscous dissipation than an all-purpose shortening, characteristics that are key hallmarks of ductile (roll-in) and brittle (all-purpose) behavior of hard materials (Macias-Rodriguez et al. 2017). The results of oscillatory rheometry agree with those of shear creep and capillary rheology which also show that laminating shortening behave as a highly viscous pastes. It was found that at stress steps $\tau_0 = 200$ Pa, a laminating shortening had a steady shear viscosity approximately one log order higher than that of an all-purpose shortening (laminating $\eta_0 = 1 \times 10^9$ Pa.s, all-purpose $\eta_0 = 2 \times 10^8$ Pa.s). As stated previously, it was also observed that a laminating shortening remained more viscous and continuous when being extruded (Fig. 8b) ($\eta, \eta_E = 10^2$-10^3 Pa.s at 10-100 s^{-1}), whereas an all-purpose shortening ruptured and flowed more easily through the capillary die so that the value of

the pressure drop substantially decreased and was not measurable with the used instrumental setup.

To rationalize the observed nonlinear mechanical response and establish function-structure relationships, we investigate both the underlying nanostructure as well as the microstructure (20 nm to 6 μm) using USAXS and SEM techniques. USAXS data informs of the mechanisms involved in particle/cluster aggregation and structural features of the network, i.e. size, morphology, mass distribution, and of the fundamental scatterers, i.e. crystal nanoplatelets (Peyronel, Quinn, et al., 2014; Pink et al., 2015). Using the Unified Fit model, three and two power laws (structural levels or hierarchies) are identified for laminating and all-purpose shortenings, respectively (Fig. 10). The high-q power law slope P_1 (level 1) indicates CNPs with smooth ($P\approx4$) and rough ($P<4$) interfaces for roll-in and all-purpose shortenings, respectively (Peyronel et al. 2014). Variations on CNPs surface morphology is attributed to higher (roll-in) and lower (all-purpose) content of trisaturated TAGs, as described by (Peyronel, Pink, et al., 2014). Remarkably, 'particle' or CNP sizes (R_{g1}) of laminating shortening are up to eleven folds smaller than those all-purpose shortening. The intermediate-power law slope P_2 (level 2) for laminating shortening, indicates self-assembly of CNPs into fractal clusters due to competition between their condensation and diffusion ($P_2>2.1$) or DLCA mechanisms ($P_2\approx1.8$). The low-q power law P_3 (level 3) suggests the presence of micrometer-scaled crystal clusters with fractally diffuse interfaces ($P_3>4$). Using the Guinier-Porod model, it was found that CNPs aggregated into mesoscopic-scale "supra-platelets" ($S = 2$) or structures intermediate between rods and platelets ($1<S<2$) (Macias-Rodriguez et al. 2017). SEM micrographs revealed homogenous and elongated microstructures composed of "multilayers" made of well-defined crystal aggregates

(~4 μm length) for laminating shortening, whereas heterogeneous networks of distorted sheet-like crystal aggregates (~4 μm length) for all-purpose shortening. Based on our rheo-structural investigation, we suggest that a laminating shortening dissipates more effectively shear loads since energy is allocated among three hierarchies in contrast to an all-purpose shortening where energy is exchanged solely between two hierarchies. In addition, the microstructure of a laminating shortening relieves better local stresses by inelastic deformation due to control sliding motion of the elongated crystal layers in which the liquid oil serves as a lubricant. These explanations seem plausible, as similar findings have been reported for biological and biological-like materials with similar constituents and volume fractions (Sen and Buehler 2011; Ritchie 2011). Furthermore, it is noted that several compositions meet the unique rheological "fingerprint", suggesting that in designing for roll-in performance the exact bulk composition (e.g., *trans* or *trans*-free oil blends, oil base stock) does not matter (Macias-Rodriguez et al. 2017)

Conclusions and perspectives

Fat viscoelasticity is imparted by the structure of the anisotropic crystal network. Significant progress has been made on structural characterization of fats, being the findings of USAXS the most recent advance. As supported by the literature, the development of the solid like network encompasses the formation of hierarchical levels affected by non-trivial thermodynamics and kinetics of crystallization. These concurring factors make the task of drawing meaningful correlations among structure, physicochemical properties and mechanical functionality of complex fats, a very difficult one. Functionality or macroscopic performance as related to linear

viscoelasticity has been extensively studied; however nonlinear viscoelasticity of fats has been scarcely investigated or at least not in a systematic fashion. At large deformations, beyond a critical strain or stress, fats yield irreversibly and display rich nonlinear behavior (i.e., softening, thixotropy) that deserve special attention given that all processing and end-uses are nonlinear flows. At a fundamental level, it is desirable to elucidate the nonlinear rheology of fats by computer simulations and time- and space- resolved rheo-scattering probes. Moreover, it is essential to understand nonlinear rheological properties in terms of mechanical contributions of each of the multiple hierarchical levels or at least relate specific mechanical functions to structure as highlighted in this review (refer to case study section). At an applied level, it is possible to define macroscopic performance in terms of unique rheological "fingerprints" to answer pragmatic questions such as "*what rheological functions and magnitudes are desirable for a good laminating shortening?.*" Such analysis is highly beneficial not only for quality control purposes, but also for reformulation of fats (no-*trans* and low-saturates) or design of alternative lipid-structuring materials (e.g., organogels) where nonlinear viscoelasticity can serve as a screening tool for targeting mechanical functionality.

References

Acevedo, N. C. and Marangoni, A. G. (2010). Characterization of the Nanoscale in Triacylglycerol Crystal Networks. *Cryst. Growth Des.* **10**: 3327–3333.

Acevedo, N. C., Peyronel, F., and Marangoni, A. G. (2011). Nanoscale structure intercrystalline interactions in fat crystal networks. *Curr. Opin. Colloid Interface Sci.* **16**: 374–383.

Atkins, A. G. and Tabor, D. (1965). Plastic indentation in metals with cones. *J. Mech. Phys. Solids* **13**: 149–164.

Bistany, K. L. and Kokini, J. L. (1983). Comparison of Steady Shear Rheological Properties and Small Amplitude Dynamic Viscoelastic Properties of Fluid Food Materials. *J. Texture Stud.* **14**: 113–124.

de Bruijne, D. W. and Bot, A. (1999). **In**: Fabricated fat-based foods., pp. 185–227 , Rosenthal,A.J. (ed)., *Food texture: measurement and perception*. Aspen Publishers, Gaithersburg.

Castro, M., Giles, D. W., Macosko, C. W., and Moaddel, T. (2010). Comparison of methods to measure yield stress of soft solids. *J. Rheol.* **54**: 81–94.

Cavillot, V., Pierart, C., Kervyn De Meerendré, M., Vincent, M., Paquot, M., Wouters, J., … Danthine, S. (2009). Physicochemical properties of European bakery margarines with and without trans fatty acids. *J. Food Lipids* **16**: 273–286.

Cho, K. S., Hyun, K., Ahn, K. H., and Lee, S. J. (2005). A geometrical interpretation of large

amplitude oscillatory shear response. *J. Rheol.* **49**: 747–758.

Christensen, R. (1982). Theory of viscoelasticity: an introduction. Academic Press, New York.

Coussot, P. (2007). Rheophysics of pastes: a review of microscopic modelling approaches. *Soft Matter* **3**: 528–540.

Davis, J. G. (1937). Extending yield stress fluid paradigms. *J. Dairy Res.* **8**: 245–264.

Dealy, J. M. and Wissbrun, K. F. Melt rheology and its role in plastic processing: theory and applications. Van Nostrand Reinhold, New York.

DeMan, J. M. and Beers, A. M. (1987). Fat crystal networks: structure and rheological properties. *J. Texture Stud.* **18**: 303–318.

DeMan, J. M., Gupta, S., Kloek, M., and Timbers, G. E. (1985). Viscoelastic properties of plastic fat products. *J. Am. Oil Chem. Soc.* **62**: 1672–1675.

DeMan, L., DeMan, J. M., and Blackman, B. (1991). Physical and Textural Characteristics of Some North American Shortenings. *J. Am. Oil Chem. Soc.* **68**: 63–69.

DeMan, L., DeMan, J. M., and Blackman, B. (1989). Physical and textural evaluation of some shortenings and margarines. *J. Am. Oil Chem. Soc.* **68**: 63–69.

DeMan, L., Shen, C. F., and DeMan, J. M. (1991). Composition , Physical and Textural Characteristics of Soft (Tub) Margarines. *J. Am. Oil Chem. Soc.* **68**: 70–73.

Dimitriou, C. J., Ewoldt, R. H., and McKinley, G. H. (2013). Describing and prescribing the constitutive response of yield stress fluids using large amplitude oscillatory shear stress

(LAOStress). *J. Rheol.* **57**: 27–70.

Ewoldt, R. H. (2013). Defining nonlinear rheological material functions for oscillatory shear. *J. Rheol.* **57**: 177–195.

Ewoldt, R. H. and Bharadwaj, N. A. (2013). Low-dimensional intrinsic material functions for nonlinear viscoelasticity. *Rheol. Acta* **52**: 201–219.

Ewoldt, R. H., Clasen, C., Hosoi, a. E., and McKinley, G. H. (2007). Rheological fingerprinting of gastropod pedal mucus and synthetic complex fluids for biomimicking adhesive locomotion. *Soft Matter* **3**: 634–643.

Ewoldt, R. H., Hosoi, A. E., and McKinley, G. H. (2008). New measures for characterizing nonlinear viscoelasticity in large amplitude oscillatory shear. *J. Rheol.* **52**: 1427–1458.

Ewoldt, R. H., Johnston, M. T., and Caretta, L. M. (2015). **In**: Experimental challenges of shear rheology : how to avoid bad data., pp. 207–241 , Spagnolie,S.E. (ed)., *Complex fluids in Biological systems*. Springer, New York.

Ewoldt, R. H. and McKinley, G. H. (2010). On secondary loops in LAOS via self-intersection of Lissajous–Bowditch curves. *Rheol. Acta* **49**: 213–219.

Ewoldt, R. H., Winter, P., Maxey, J., and McKinley, G. H. (2010). Large amplitude oscillatory shear of pseudoplastic and elastoviscoplastic materials. *Rheol. Acta* **49**: 191–212.

Ferry, J. D. (1980). Viscoelastic properties of polymers. Wiley, New York.

Fine, F. B., Paska, J. M., and Feeny, J. F. (2006). Low trans puff pastry composition, method of

ACCEPTED MANUSCRIPT

use and puff pastry products.

Garcia-Macias, P., Gordon, M. H., Frazier, R. A., Smith, K., and Gambelli, L. (2012). Effect of TAG composition on performance of low saturate shortenings in puff pastry. *Eur. J. Lipid Sci. Technol.* **114**: 741–747.

Garcia-Macias, P., Gordon, M. H., Frazier, R. A., Smith, K. S., and Gambelli, L. (2011). Performance of palm-based fat blends with a low saturated fat content in puff pastry. *Eur. J. Lipid Sci. Technol.* **113**: 1474–1480.

Ghotra, B. S., Dyal, S. D., and Narine, S. S. (2002). Lipid shortenings: a review. *Food Res. Int.* **35**: 1015–1048.

Giacomin, A. J. and Dealy, J. M. (1993). **In**: Large amplitude oscillatory shear., pp. 99–121 , Collyer,A.A. (ed)., *Techniques in rheological measurement*. Springer Netherlands.

Giacomin, A. J., Gilbert, P. H., Merger, D., and Wilhelm, M. (2015). Large-amplitude oscillatory shear: comparing parallel-disk with cone-plate flow. *Rheol. Acta* **54**: 263–285.

Gonzalez-Gutierrez, J. and Scanlon, M. G. (2013). Strain Dependence of the Uniaxial Compression Response of Vegetable Shortening. *J. Am. Oil Chem. Soc.* **90**: 1319–1326.

Haighton, A. J. (1959). The measurement of the hardness of margarine and fats with cone penetrometers. *J. Am. Oil Chem. Soc.* **36**: 345–348.

Haighton, A. J. (1965). Worksoftening of Margarine and Shortening. *J. Am. Oil Chem. Soc.* **42**: 27–30.

Hayakawa, M. and DeMan, J. M. (1982). Interpretation of Cone Penetrometer Consistency Measurements of Fats. *J. Texture Stud.* **13**: 201–210.

Heertje, I. (1993). Microstructural studies in fat research. *Food Struct.* **12**: 77–94.

Heng, P. W. S., Chan, L. W., and Chow, K. T. (2005). Development of novel nonaqueous ethylcellulose gel matrices: rheological and mechanical characterization. *Pharm. Res.* **22**: 676–84.

Himawan, C., Starov, V. M., and Stapley, A. G. F. (2006). Thermodynamic and kinetic aspects of fat crystallization. *Adv. Colloid Interface Sci.* **122**: 3–33.

Hyun, K., Kim, S. H., Ahn, K. H., and Lee, S. J. (2002). Large amplitude oscillatory shear as a way to classify the complex fluids. *J. Nonnewton. Fluid Mech.* **107**: 51–65.

Hyun, K., Wilhelm, M., Klein, C. O., Soo, K., Gun, J., Hyun, K., … McKinley, G. H. (2011). Progress in Polymer Science A review of nonlinear oscillatory shear tests : Analysis and application of large amplitude oscillatory shear (LAOS). *Prog. Polym. Sci.* **36**: 1697–1753.

Juriaanse, A. C. and Heertje, I. (1988). Microstructure of shortenings, margarine and butter-A review. *Food Microstruct* **7**: 181–188.

Kim, J., Merger, D., Wilhelm, M., and Helgeson, M. E. (2014). Microstructure and nonlinear signatures of yielding in a heterogeneous colloidal gel under large amplitude oscillatory shear. *J. Rheol.* **58**: 1359–1390.

Kloek, W., Vliet, T. V., and Walstra, P. (2005). Mechanical properties of fat dispersions

prepared in a mechanical crystallizer. *J. Texture Stud.* **36**: 544–568.

Kulkarni, C. V. (2012). Lipid crystallization: from self-assembly to hierarchical and biological ordering. *Nanoscale* **4**: 5779–5791.

Läuger, J. and Stettin, H. (2010). Differences between stress and strain control in the non-linear behavior of complex fluids. *Rheol. Acta* **49**: 909–930.

Li, X., Wang, S.-Q., and Wang, X. (2009). Nonlinearity in large amplitude oscillatory shear (LAOS) of different viscoelastic materials. *J. Rheol.* **53**: 1255–1274.

Macias-Rodriguez, B., Ewoldt, R. H., and Marangoni, A. G. (2017). Nonlinear viscoelasticity of fats.Under review.

Macias-Rodriguez, B. and Marangoni, A. G. (2016a). Physicochemical and Rheological Characterization of Roll-in Shortenings. *J. Am. Oil Chem. Soc.* **93**: 575–585.

Macias-Rodriguez, B. and Marangoni, A. G. (2016b). Rheological characterization of triglyceride shortenings. *Rheol. Acta* **55**: 767–779.

Macosko, C. W. (1994). Rheology: principles, measurements and applications. Wiley, New York.

Mao, B., Divoux, T., and Snabre, P. (2016). Normal force controlled rheology applied to agar gelation. *J. Rheol.* **60**: 473–489.

Marangoni, A. G. (2000). Elasticity of high-volume-fraction fractal aggregate networks: A thermodynamic approach. *Phys. Rev. B - Condens. Matter Mater. Phys.* **62**: 13951–13955.

Marangoni, A. G., Acevedo, N. C., Maleky, F., Co, E., Peyronel, F., Mazzanti, G., … Pink, D. A. (2012). Structure and functionality of edible fats. *Soft Matter* **8**: 1275.

Marangoni, A. G. and Narine, S. S. (2002). Identifying key structural indicators of mechanical strength in networks of fat crystals. *Food Res. Int.* **35**: 957–969.

Marangoni, A. G. and Pink, D. A. (2014). Edible nanostructures: A bottom-up Approach.

Marangoni, A. G. and Rogers, M. A. (2003). Structural basis for the yield stress in plastic disperse systems. *Appl. Phys. Lett.* **82**: 3239–3241.

Marangoni, A. G. and Rousseau, D. (1996). Is plastic fat rheology governed by the fractal nature of the fat crystal network? *J. Am. Oil Chem. Soc.* **73**: 991–994.

Mensink, R. P., Zock, P. L., and Katan, M. B. (2003). Effects of dietary fatty acids and carbohydrates on the ratio of serum total to HDL cholesterol and on serum lipids and apolipoproteins : a meta-analysis of 60 controlled trials. *Am. J. Clin. Nutr.* **77**: 1146–1155.

Mensink, R. P., Zock, P. L., Katan, M. B., and Affiliations, A. (2003). Effects of dietary fatty acids and carbohydrates on the ratio of serum total to HDL cholesterol and on serum lipids and apolipoproteins : a meta- - analysis of 60. *Am. J. Clin. Nutr.* **77**: 1146–1155.

Merger, D. and Wilhelm, M. (2014). Intrinsic nonlinearity from LAOStrain—experiments on various strain- and stress-controlled rheometers: a quantitative comparison. *Rheol. Acta* **53**: 621–634.

Min Kim, J., Eberle, A. P. R., Kate Gurnon, a., Porcar, L., and Wagner, N. J. (2014). The

microstructure and rheology of a model, thixotropic nanoparticle gel under steady shear and large amplitude oscillatory shear (LAOS). *J. Rheol.* **58**: 1301–1328.

Morales-Rueda, J. A., Dibildox-Alvarado, E., Charó-Alonso, M. A., and Toro-Vazquez, J. F. (2009). Rheological Properties of Candelilla Wax and Dotriacontane Organogels Measured with a True-Gap System. *J. Am. Oil Chem. Soc.* **86**: 765–772.

Mozaffarian, D., Katan, M. B., Ascherio, A., Stampfer, M. J., and Willett, W. C. (2006). Trans fatty acids and cardiovascular disease. *N. Engl. J. Med.* **354**: 1601–1613.

Narine, S. S. and Marangoni, A. G. (1999a). Fractal nature of fat crystal networks. *Phys. Rev. E* **59**: 1908–1920.

Narine, S. S. and Marangoni, A. G. (1999b). Mechanical and structural model of fractal networks of fat crystals at low deformations. *Phys. Rev. E. Stat. Phys. Plasmas. Fluids. Relat. Interdiscip. Topics* **60**: 6991–7000.

Narine, S. S. and Marangoni, A. G. (1999c). Microscopic and rheological studies of fat crystal networks. *J. Cryst. Growth* **198–199**: 1315–1319.

Narine, S. S. and Marangoni, A. G. (1999d). Relating structure of fat crystal networks to mechanical properties: A review. *Food Res. Int.* **32**: 227–248.

Ooms, N., Pareyt, B., Brijs, K., and Delcour, J. A. (2015). Ingredient Functionality in Multilayered Dough-margarine Systems and the Resultant Pastry Products: A Review. *Crit. Rev. Food Sci. Nutr.* **8398**: 00–00.

Pajin, B., Šoronja-Simović, D., Šereš, Z., Gyura, J., Radujko, I., and Sakač, M. (2011). Physicochemical and textural properties of puff pastry margarines. *Eur. J. Lipid Sci. Technol.* **113**: 262–268.

Petekidis, G. (2014). Rheology of colloidal gels. *J. Rheol.* **58**: 1085–1087.

Peyronel, F., Ilavsky, J., Mazzanti, G., Marangoni, A. G., and Pink, D. A. (2013). Edible oil structures at low and intermediate concentrations. II. Ultra-small angle X-ray scattering of in situ tristearin solids in triolein. *J. Appl. Phys.* **114**: 234902.

Peyronel, F., Pink, D. A., and Marangoni, A. G. (2014). Triglyceride Nanocrystal Aggregation into Polycrystalline Colloidal Networks: Ultra-Small Angle X-Ray Scattering, Models and Computer Simulation. *Curr. Opin. Colloid Interface Sci.* **19**: 459–470.

Peyronel, F., Quinn, B., Marangoni, A. G., and Pink, D. A. (2014). Ultra small angle x-ray scattering in complex mixtures of triacylglycerols. *J. Phys. Condens. Matter* **26**: 464110.

Pink, D. A., Peyronel, F., Quinn, B., Singh, P., and Marangoni, A. G. (2015). Condensation versus diffusion. A spatial-scale-independent theory of aggregate structures in edible oils: applications to model systems and commercial shortenings studied via rheology and USAXS. *J. Phys. D. Appl. Phys.* **48**: 384003.

Pink, D. A., Quinn, B., Peyronel, F., and Marangoni, A. G. (2013). Edible oil structures at low and intermediate concentrations. I. Modeling, computer simulation, and predictions for X ray scattering. *J. Appl. Phys.* **114**: 234901.

Pipkin, A. C. (1972). Lectures on viscoelasticity theory Second edition. 2nd ed. Springer-

Verlag, New York.

Quinn, B., Peyronel, F., Gordon, T., Marangoni, A., Hanna, C. B., and Pink, D. A. (2014). Aggregation in complex triacylglycerol oils: coarse-grained models, nanophase separation, and predicted x-ray intensities. *J. Phys. Condens. Matter* **26**: 464108.

Renou, F., Stellbrink, J., and Petekidis, G. (2010). Yielding processes in a colloidal glass of soft star-like micelles under large amplitude oscillatory shear (LAOS). *J. Rheol.* **54**: 1219.

Ritchie, R. O. (2011). The conflicts between strength and toughness. *Nat. Mater.* **10**: 817–822.

Rogers, S. A. (2012). A sequence of physical processes determined and quantified in (LAOS): An instantaneous local 2D/3D approach. *J. Rheol.* **56**: 1129–1151.

Rogers, S. A., Erwin, B. M., Vlassopoulos, D., and Cloitre, M. (2011). A sequence of physical processes determined and quantified in LAOS: Application to a yield stress fluid. *J. Rheol.* **55**: 435–458.

Rohm, H. and Weidinger, K. H. (1993). Rheological Behaviour of Butter At Small Deformations. *J. Texture Stud.* **24**: 157–172.

Sato, K. (2001). Crystallization behaviour of fats and lipids — a review. *Chem. Eng. Sci.* **56**: 2255–2265.

Sato, K. and Ueno, S. (2011). Current Opinion in Colloid & Interface Science Crystallization , transformation and microstructures of polymorphic fats in colloidal dispersion states. *Curr. Opin. Colloid Interface Sci.* **16**: 384–390.

Scott Blair, G. W. (1954). The rheology of fats: a review. *J. Sci. Food Agric.* **5**: 401–405.

Scott Blair, G. W. (1938). The spreading capacity of butter. I. *J. Dairy Res.* **9**: 208–214.

Scott Blair, G. W. and Burnett, J. (1959). On the creep, recovery, relaxation and elastic "memory" of some renneted milk gels. *Br. J. Appl. Phys.* **10**: 15–20.

Sen, D. and Buehler, M. J. (2011). Structural hierarchies define toughness and defect-tolerance despite simple and mechanically inferior brittle building blocks. *Sci. Rep.* **1**: 1–9.

Shama, F. and Sherman, P. (1970). the Influence of Work Softening on the Viscoelastic Properties of Butter and Margarine. *J. Texture Stud.* **1**: 196–205.

Sone, T. (1961). The rheological behavior and thixotropy of a fatty plastic body. *J. Phys. Soc. Japan* **16**: 961–971.

Steffe, J. F. (1996). Rheological Methods in Food Processing Engineering. Freeman press, East Lansing.

Szczesniak, A. S. (2002). Texture is a sensory property. *Food Qual. Prefer.* **13**: 215–225.

Tang, D. and Marangoni, A. G. (2007). Modeling the rheological properties and structure of colloidal fat crystal networks. *Trends Food Sci. Technol.* **18**: 474–483.

Tang, D. and Marangoni, A. G. (2006). Quantitative study on the microstructure of colloidal fat crystal networks and fractal dimensions. *Adv. Colloid Interface Sci.* **128–130**: 257–265.

van den Tempel, M. (1961). Mechanical properties of plastic-disperse systems at very small deformations. *J. Colloid Sci.* **16**: 284–296.

van den Tempel, M. (1979). Rheology of Concentrated Suspensions. *J. Colloid Interface Sci.* **71**: 18–20.

van den Tempel, M. (1958). Rheology of plastic fats. *Rheol. Acta* **1**: 115–118.

Thareja, P. (2013). Rheology and microstructure of pastes with crystal network. *Rheol. Acta* **52**: 515–527.

Thareja, P., Golematis, A., Street, C. B., Wagner, N. J., Vethamuthu, M. S., Hermanson, K. D., and Ananthapadmanabhan, K. P. (2013). Influence of surfactants on the rheology and stability of crystallizing fatty acid pastes. *J. Am. Oil Chem. Soc.* **90**: 273–283.

Thareja, P., Street, C. B., Wagner, N. J., Vethamuthu, M. S., Hermanson, K. D., and Ananthapadmanabhan, K. P. (2011). Development of an in situ rheological method to characterize fatty acid crystallization in complex fluids. *Colloids Surfaces A Physicochem. Eng. Asp.* **388**: 12–20.

Tschoegl, N. W. (1989). The phenomenological theory of linear viscoelastic behavior: An introduction. Springer-Verlag, Berlin.

Uauy, R., Aro, A., Clarke, R., Ghafoorunissa, R., L 'abbé, M., Mozaffarian, D., … Tavella, M. (2009). WHO Scientific Update on trans fatty acids: summary and conclusions. *Eur. J. Clin. Nutr.* **63**: 68–75.

Vreeker, R., Hoekstra, L. L., den Boer, D. C., and Agterof, W. G. M. (1992). The fractal nature of fat crystal networks. *Colloids and Surfaces* **65**: 185–189.

Wilhelm, M. (2002). Fourier-Transform Rheology. *Macromol. Mater. Eng.* **287**: 83–105.

Zhong, Y. and Wang, S.-Q. (2003). Exfoliation and yield behavior in nanodispersions of organically modified montmorillonite clay. *J. Rheol.* **47**: 483–495.
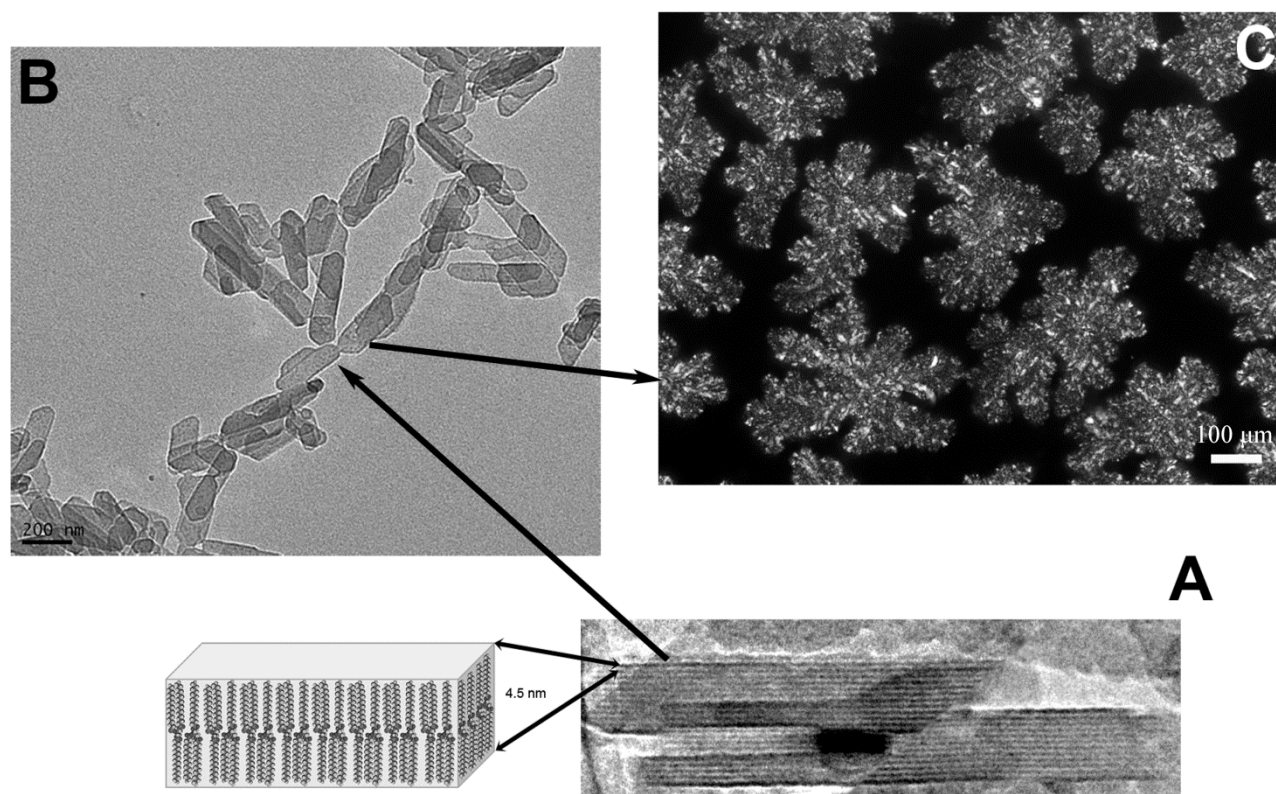
Fig. 1 The hierarchical structure of fat materials. (a) TEM micrograph of epitaxial stacking of crystal lamellae form a nanoplatelet (side view). Left side: schematic representation of an individual crystal lamellae illustrating side-to-side packing of pairs of TAGs, each TAG is in a tuning fork conformation. (b) Top view of crystal nanoplatelets. (c) Polarized-light micrograph of the fat microstructure (birefringent) embedded in liquid oil (dark).
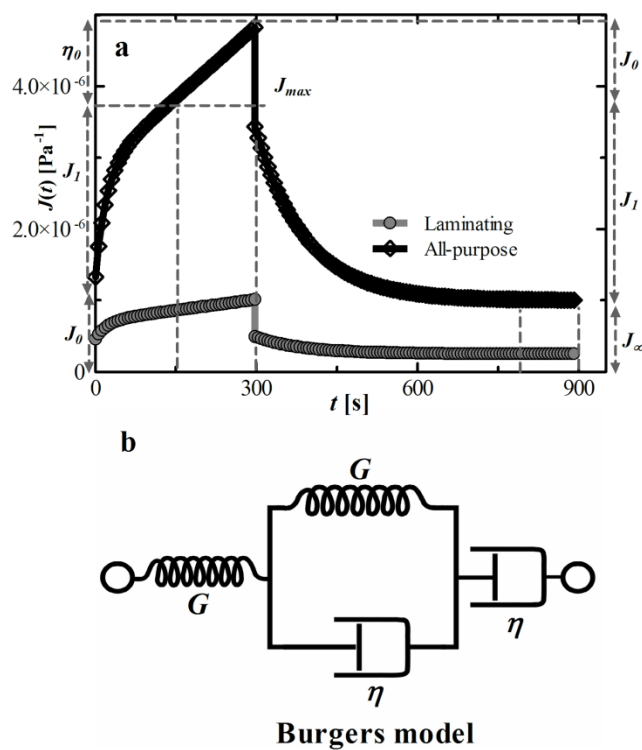
Fig. 2 (a) Creep and recovery curve of laminating and all-purpose shortenings. Dotted gray lines indicate viscoelastic parameters and time intervals used by the Burgers model (b).
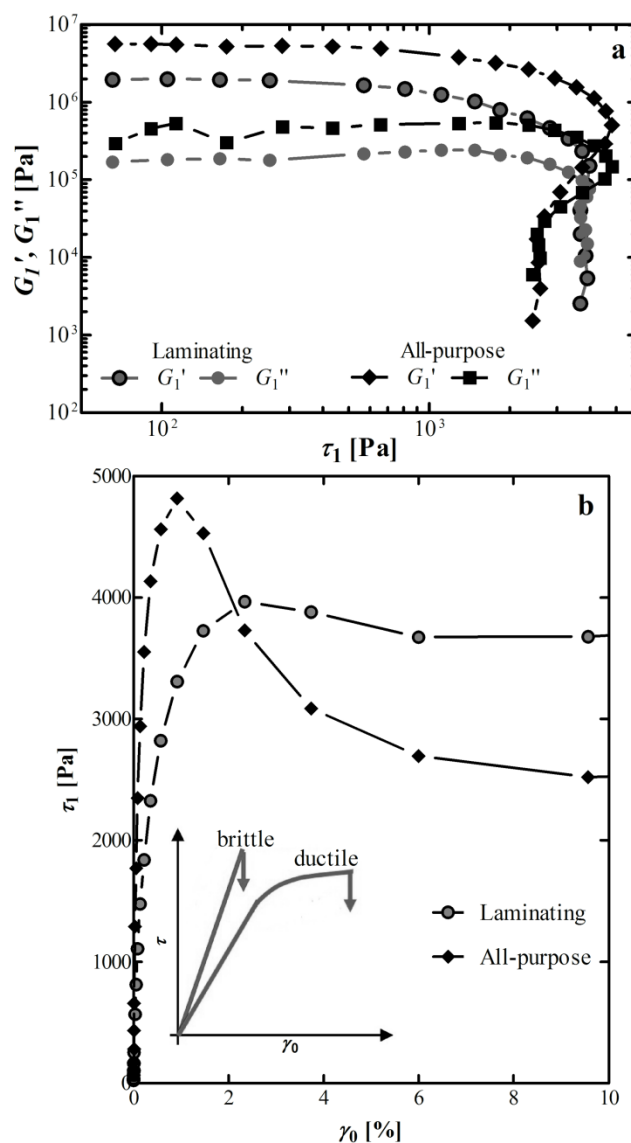
Fig. 3 (a) Elastic G' and viscous G'' moduli as a function of stress as procured from a strain amplitude sweep ($\gamma_0 = 0.01\text{-}100\%$, $\omega = 3.6$ rads^{-1}). (b) Stress versus strain plots of laminating and all-purpose shortenings. Inset denotes ideal ductile and brittle solid behavior.
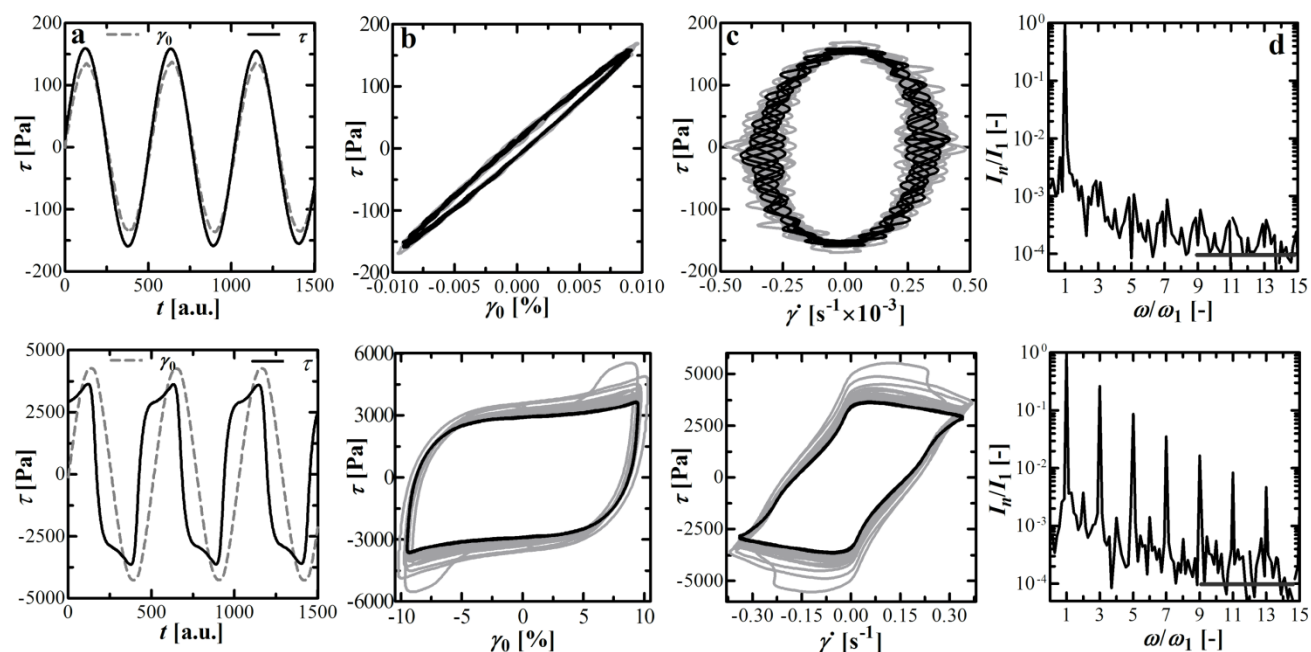
Fig. 4 (a) Stress (full black lines) and strain (dotted gray lines) waveforms versus time. Raw Lissajous-Bowditch plots of (b) stress versus strain (elastic representation) and (c) stress versus shear rate (viscous representation). The gray lines correspond to transients, whereas the solid black lines represent the steady state data. (d) frequency-domain Fourier spectra. The data on the top row were collected in the SAOS regime ($\gamma_0 = 0.01\%$), whereas the data on the down row were obtained in the LAOS regime ($\gamma_0 = 10\%$), for a laminating shortening at T = 16°C.
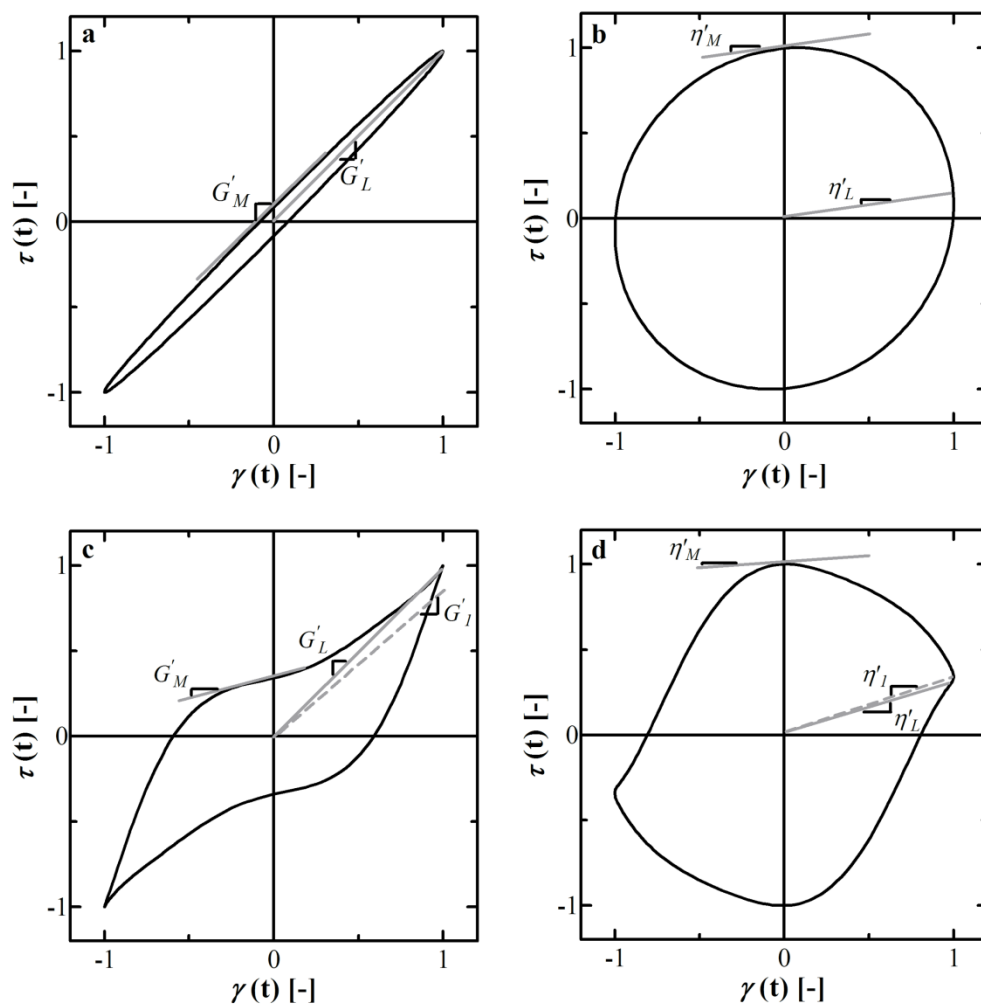
Fig. 5 Definitions of material measures as proposed by (Ewoldt et al., 2008), for reporting viscoelastic moduli: (a),(b) elastic moduli and dynamic viscosities, respectively, for a model linear viscoelastic response at $\{\omega = 3.59 \text{ rad s}^{-1}, \gamma_0 = 0.01\}$; (c),(d) elastic moduli and dynamic viscosities, respectively, for a nonlinear viscoelastic response at $\{\omega = 3.59 \text{ rad s}^{-1}, \gamma_0 = 1.34\%\}$. The first harmonic moduli are shown for comparison. In the linear regime [(a),(b)] all measures are equivalent to the linear viscoelastic moduli. A nonlinear material response [(c),(d)] will result in different values for each material measure. All the shown data were measured for an all-purpose shortening at T = 16°C.
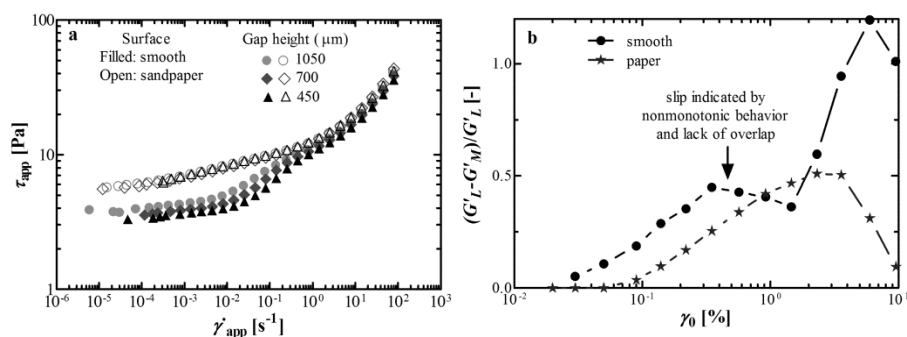
Fig. 6 (a) Wall slip on a smooth surface and elimination of wall slip on a sandpapered surface, respectively, for a water-in-oil emulsion (Nivea Lotion) tested using parallel plates of diameter D = 40 mm at multiple gaps h = 450-1050 μm. Adapted from Ewoldt et al., (2015). (b) Wall slip on a custom sandblasted surface and absence of wall slip on a filter-paper surface, respectively, in a cake shortening using parallel plates of diameter D = 20 mm at a fixed gap h = 1300 μm.
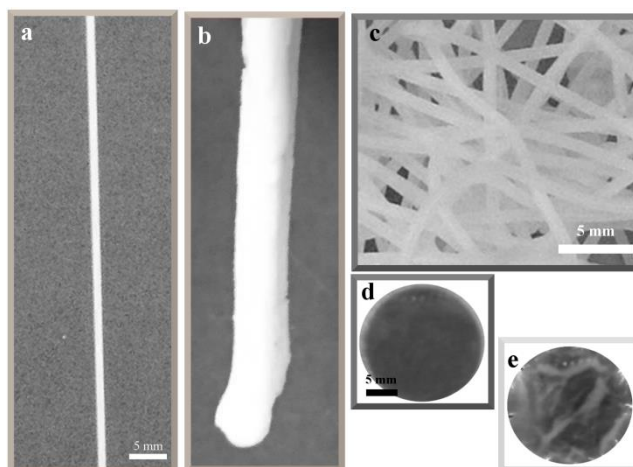
Fig. 7 Macroscopic appearance of laminating and all-purpose shortenings. (a) laminating and (b) all-purpose shortening, during capillary flow. (a) and (b) share the same scale bar. (c) "entangled" threads of laminating shortening collected at the exit of capillary rheometer. (d) laminating and (e) all-purpose shortenings, after compression. (d) and (e) share the same scale bar.
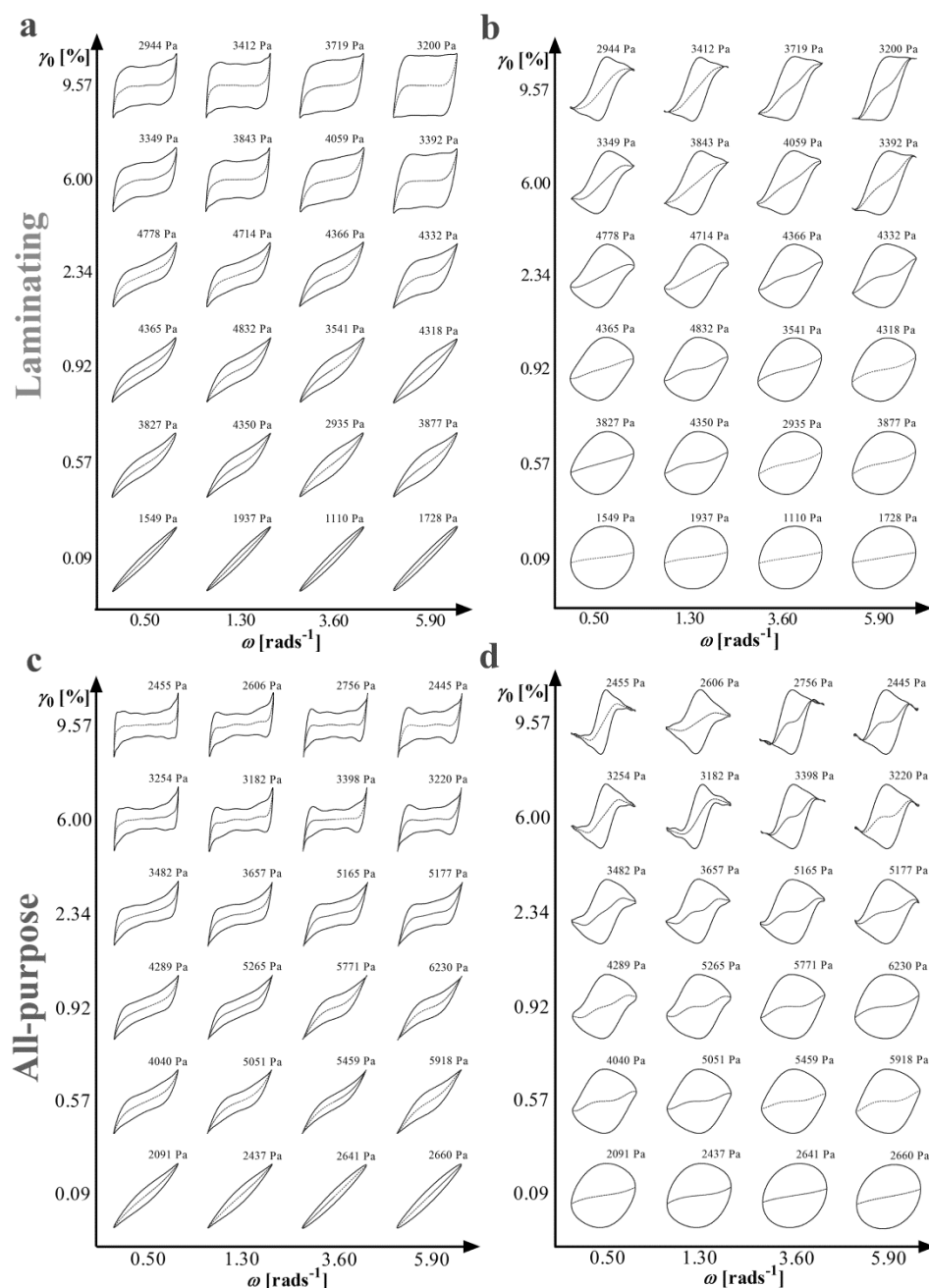
Fig. 8 Normalized elastic (a, c) and viscous (b, d) Lissajous-Bowditch curves collapsed in a

Pipkin space at the corresponding input parameters of frequency and strain-amplitude.

Continuous shapes correspond to the total stress, whereas lines contained inside the figures

represent the decomposed elastic and viscous stress, respectively. The maximum stress τ_{max} in each test is shown above each limit cycle. (a, b) laminating and (c, d) all-purpose shortenings.
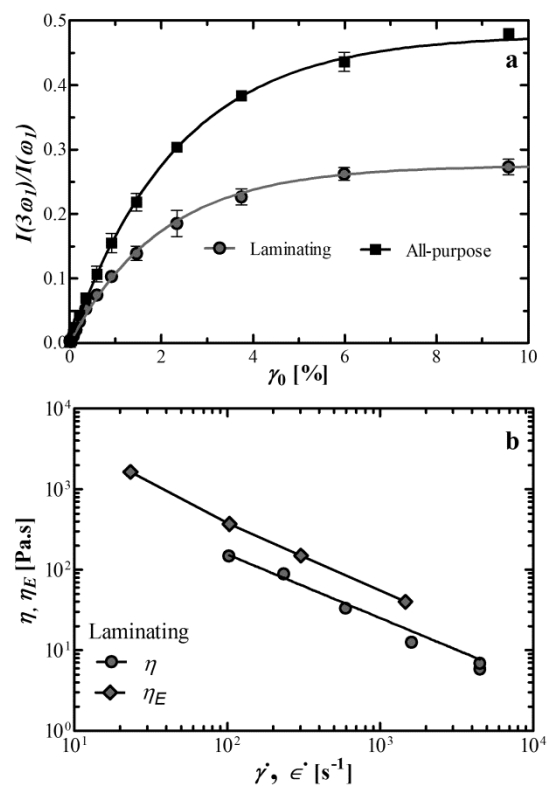
Fig. 9 a) Third-order harmonic of laminating and all-purpose shortenings as obtained from

LAOS experiments at $\omega = 3.6$ rads^{-1}. b) Shear and elongational viscosity as determined from

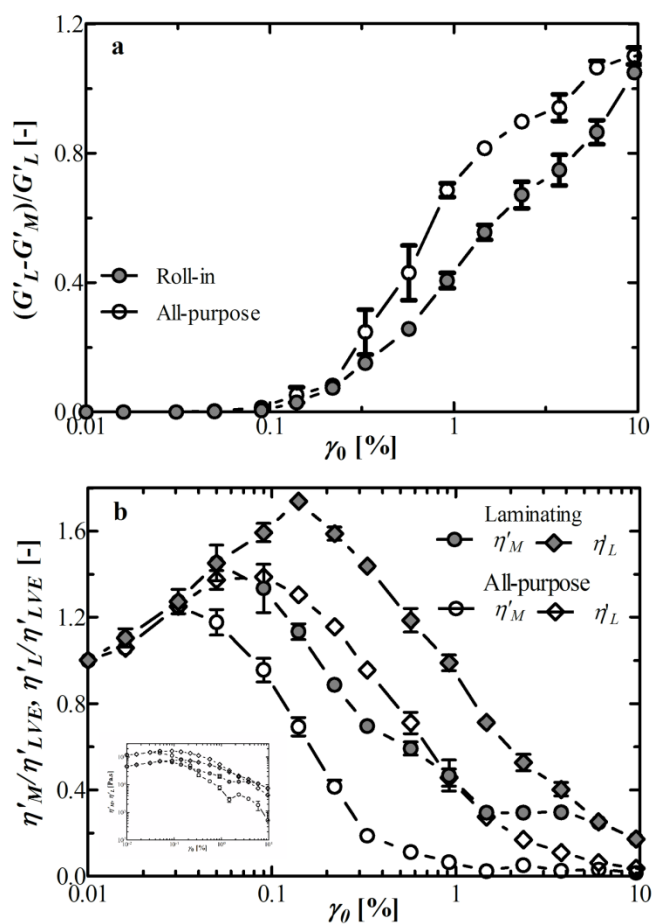entrance pressure and pressure drops measured by capillary rheometer.

Fig. 10 Nonlinear a) Elastic and b) viscous measures for laminating and all-purpose shortenings as calculated from LAOS data at $\omega = 3.6$ rads^{-1}. (b) Measures are parametrized by the linear dynamic viscosity η_{LVE}' at $\gamma_0 = 0.01\%$, inset shows absolute values of dynamic viscosities.
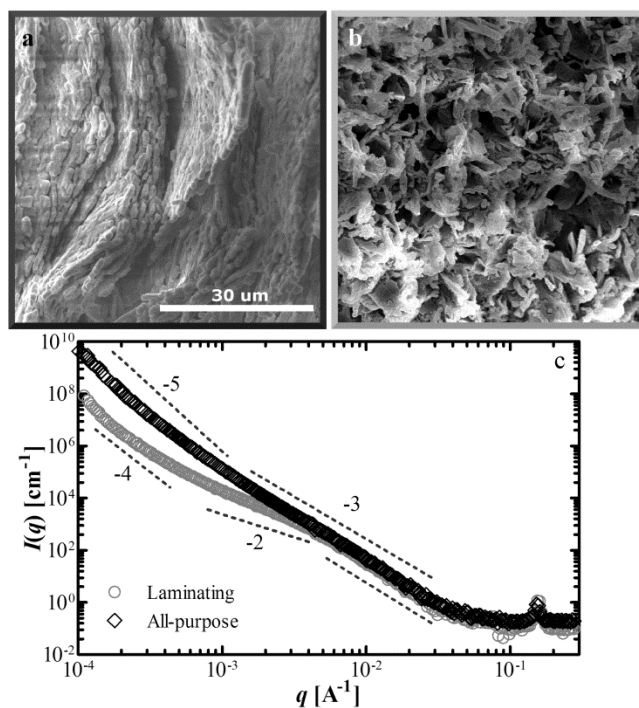
Fig. 11 Microscopic-to-nanoscopic structure of (a) laminating and (b) all-purpose shortenings as probed by SEM and USAXS. SEM images (a,b) share the same magnification bar. Dotted lines in the USAXS plots (c) serve as 'guides to the eyes'.